MODELING ACTION POTENTIAL PROPAGATION DURING HYPERTROPHIC CARDIOMYOPATHY THROUGH A THREE-DIMENSIONAL COMPUTATIONAL MODEL

A Thesis

presented to

the Faculty of California Polytechnic State University,

San Luis Obispo

In Partial Fulfillment

of the Requirements for the Degree

Master of Science in Biomedical Engineering

by

Julia Kelley

June 2021

COMMITTEE MEMBERSHIP

TITLE:	Modeling Action Potential Propagation During Hypertrophic Cardiomyopathy Through a Three-Dimensional Computational Model
AUTHOR:	Julia Kelley
DATE SUBMITTED:	June 2021
COMMITTEE CHAIR:	Robert Szlavik, Ph.D. Professor of Biomedical Engineering
COMMITTEE MEMBER:	David Clague, Ph.D. Professor of Biomedical Engineering
COMMITTEE MEMBER:	Michael Whitt, Ph.D. Professor of Biomedical Engineering

ABSTRACT

Modeling Action Potential Propagation During Hypertrophic Cardiomyopathy Through a Three-Dimensional Computational Model

Julia Kelley

Hypertrophic cardiomyopathy (HCM) is the most common monogenic disorder and the leading cause of sudden arrhythmic death in children and young adults. It is typically asymptomatic and first manifests itself during cardiac arrest, making it a challenge to diagnose in advance. Computational models can explore and reveal underlying molecular mechanisms in cardiac electrophysiology by allowing researchers to alter various parameters such as tissue size or ionic current amplitudes. The goal of this thesis is to develop a computational model in MATLAB and to determine if this model can accurately indicate cases of hypertrophic cardiomyopathy. This goal is achieved by combining a three-dimensional network of the bidomain model with the Beeler-Reuter model and then by manually varying the thickness of that tissue and recording the resulting membrane potential with respect to time. The results of this analysis demonstrated that the developed model is able to depict variations in tissue thickness through the difference in membrane potential recordings. A one-way ANOVA analysis confirmed that the membrane potential recordings of the different thicknesses were significantly different from one another. This study assumed continuum behavior, which may not be indicative of diseased tissue. In the future, such a model might be validated through in vitro experiments that measure electrical activity in hypertrophied cardiac tissue. This model may be useful in future applications to study the ionic mechanisms related to hypertrophic cardiomyopathy or other related cardiac diseases.

Keywords: Hypertrophic Cardiomyopathy, Beeler Reuter, Bidomain, computational modeling

ACKNOWLEDGMENTS

Thank you to:

- Dr. Szlavik for his support and guidance
- Dr. Clague and Dr. Whitt for serving on my committee
- Dr. Eason for his assistance with creating my model
- My parents, Mark and Jennifer, for their love and encouragement

TABLE OF CONTENTS

LIST OF TABLES

LIST OF FIGURES

Chapter 1

INTRODUCTION

The human heart is the sole organ that maintains the proper function of all other organs within the body. As the heart pumps blood throughout the body, it enables us to breathe, think, move, and empowers us in several other ways that bring quality to our lives. This quality of life is impeded at the onset of a cardiac disease, such as hypertrophic cardiomyopathy (HCM). As the leading cause of sudden arrhythmic death for children and young adults, HCM is often asymptomatic and first presents itself during ventricular tachyarrhythmia, making it impossible to diagnose before it becomes fatal. The cardiac action potential, an electrical impulse that disperses throughout the heart via rapid changes in the membrane potential of cardiomyocytes, is known to showcase evidence of HCM in its prolonged repolarization period. Computational modeling allows us to model such electrical activity within the heart. The goal of this thesis is to determine whether a three-dimensional computational model of cardiac tissue can mimic hypertrophic cardiomyopathy by varying the tissue thickness to observe changes in the shape of the action potential as it propagates through the tissue.

1.1 Motivation

Hypertrophic cardiomyopathy (HCM) is a disease that affects ventricular functioning through the increase in thickness of the ventricular wall. It is the most common monogenic cardiac disorder and is the main cause of sudden cardiac death in children and young adults [1]. Its reported prevalence is 1 in 500 adults in the U.S. and typically those who are affected are asymptomatic. It can be characterized by the unexplained thickening of the left ventricle. Mechanical stretch, caused by volume or pressure overload, leads the heart to send out stress signals which activate a hypertrophic response to compensate for wall stress. This in turn leads to cardiac remodeling [2]. The hypertrophic remodeling of the heart has three stages: developing hypertrophy, compensatory hypertrophy, and overt heart failure. In developing hypertrophy, the

load placed on the heart begins to exceed its output. In compensatory hypertrophy, the workload-to-mass ratio becomes normalized, and a resting cardiac output is maintained. Hypertrophy that occurs as a consequence of pressure overload is termed “compensatory” on the premise that it facilitates ejection performance by normalizing systolic wall stress [3]. In overt heart failure, ventricular dilation occurs and there are substantial declines in cardiac output, often leading to sudden cardiac death [3]. In fact, the first known manifestation of hypertrophic cardiomyopathy is arrhythmic sudden death caused by ventricular tachyarrhythmias [1]. HCM is challenging to diagnose since it presents as asymptomatic and doesn’t become apparent until those who are affected by it are in cardiac arrest.

The underlying electrophysiological mechanisms that cause hypertrophic cardiomyopathy are still unclear. Previous studies have investigated the ionic mechanisms driving repolarization abnormalities in human HCM cardiomyocytes. One study used experimental ionic current, action potential, and calcium-transient recordings to construct populations of human non-diseased and HCM action potential (AP) models which were then run through simulations of several degrees of selective and combined current block [1]. Another study used human embryonic stem-cell derived cardiomyocytes (hESC-CMs) subjected to mechanical stretch to investigate whether this type of in vitro model could reveal molecular mechanisms of cardiac hypertrophy and identify potential targets in the process [2]. While this model was able to replicate all specific hypertrophic hallmarks, human in vitro models are limited by the amount of available patient-derived cardiomyocytes. Likewise, animal models do not always accurately represent the mechanisms responsible for hypertrophic cardiomyopathy in humans due to inter-species differences.

Understanding the underlying electrophysiological mechanisms of hypertrophic cardiomyopathy is critical for advancing interventional therapeutics. Adequate research models are needed for the studies of root mechanisms of HCM at the molecular level. This thesis proposes combining the bidomain model with an ionic current model to create a piece of cardiac tissue for the purpose of analyzing the effects of HCM. Using a computational model to investigate how a cardiac action potential changes due to hypertrophic cardiomyopathy will be useful as it allows the researcher to vary the model parameters and observe their consequent

effects on the tissue. By taking control of the parameters that influence the cardiac action potential, one can gain insight into the root mechanisms that alter the shape of the action potential at the molecular level. Computational models may help to improve future interventional methods by providing a non-invasive, efficient method for observing changes in the action potential of cardiomyocytes that are seeded in cellular chemistry.

1.2 Previous Work

There is little information published on using in silico, or computational, models to observe the theoretical behavior of hypertrophic cardiomyopathy. A distinct divide exists in the published literature between studies that examine ionic mechanisms of hypertrophic cardiomyopathy through in vitro experiments and studies that investigate the general electrophysiological behavior of non-diseased cardiac tissue through in silico models. Previous studies [1, 2, 4] have demonstrated that ionic mechanisms significantly contribute to rhythm abnormalities. Repolarization abnormalities are particularly prominent in the case of hypertrophic cardiomyopathy [1]. Specifically, phases two and three of the action potential are prolonged. This consequence was found to be driven by L-type Ca^{2+}current reactivation [1]. Molecular mechanisms of HCM have been revealed through in vitro experiments that were additionally able to uncover biomarkers that indicated the presence of HCM [2]. Such biomarkers have not been thoroughly researched but could be a key player in developing pharmacological treatments for HCM. There have been several studies [4, 5, 6, 7] that utilized in silico modeling to look at electrical activity of the heart through a coupling of the bidomain model with an ionic current model. Multiple ionic current models have been used in the literature due to their variations in complexity. However, these studies have noted that the combination of the bidomain model with a complex ionic current model makes the simulations computationally expensive and often require great computing power [4, 7]. Another limitation of in silico models is that they often assume continuum behavior, which may not be accurate when modeling diseased tissue. Computational

modeling studies seek to characterize and predict the biophysical phenomena underlying electrical excitation and conduction [5].

A study by Passini et al. [1] used experimental ionic current, action potential, and calcium-transient recordings to construct populations of human non-diseased and HCM AP models which were subjected to simulations of several degrees of selective and combined inward current block. Passini et al. found that the simulated HCM cardiomyocytes exhibited prolonged action potentials and calcium-transient currents, along with diastolic calcium overload and a decreased calcium-transient amplitude. HCM is characterized in part by repolarization abnormalities, and this study found that while it was driven by L-type Ca^{2+} current reactivation, multichannel block increased efficacy in normalizing the repolarization as well as action potential biomarkers. While there are only a few studies that delve into researching HCM biomarkers, the ones that have researched them serve as great potential for paving the way towards treatment. A study by Ovchinnikova et al. [2] used human embryonic stem-cell derived cardiomyocytes (hESC-CMs) that were subjected to mechanical stretch to investigate whether this type of in vitro model could reveal molecular mechanisms of cardiac hypertrophy and identify potential biomarkers in the process. After subjected the hESC-CMs to cyclic mechanical stress, Ovchinnikova et al. used an RNA-sequence approach to determine the global gene expression changes involved in the hypertrophic response to stress. Genetic mutations are often a contributing factor when it comes to hypertrophic cardiomyopathy [8]. This study demonstrated the successful use of hESC-CMs in predicting molecular mechanisms of cardiac hypertrophy and identifying potential targets in the process. Ovchinnikova et al. intended to pave a way towards bridging the gap between in vitro and pharmacological approaches to understanding what causes cardiac hypertrophy.

Previous computational-based studies have been used to analyze how an electrical impulse propagates through healthy cardiac tissue by varying ionic parameters. In a study by Ibrahim et al. [4], a model composed of a bidomain coupled with the Fitzhugh-Nagumo model was implemented to study the effects of varying ionic current model parameters on the propagation of electrical waves through cardiac tissue. The model was time-discretized using the explicit forward Euler's method and space-discretized using a two-dimensional network to obtain

linearized equations. This study discovered that only a decrease in the excitation rate constants had an impact on the cardiac wave propagation. A key takeaway from Ibrahim's study is that the simulation of bidomain equations may be more fruitful if one were to use a three-dimensional network with other ionic current models. A study by Bantle [7] took the three-dimensional bidomain network approach coupled with the Ten Tusscher model [36]. Bantle, however, was unable to recreate a full action potential of a ventricular myocyte. The limitation in this result was thought to have been seeded in the coupling of neighbor cells, although it is a less accurate model when the neighboring cells are decoupled. Akin to the study by Ibrahim et al., a study by Tanyous [6] used two-dimensional bidomain modeling coupled with the Fitzhugh-Nagumo model, but instead focused on mapping electrical propagation in the cardiac sinoatrial node. The computational model was used to validate experimental treatments within the same study. Tanyous discovered that there were preferred paths of wave propagation and an uneven distribution of the velocity of wave propagation, and therefore of tissue conductance, from the sinoatrial node to its periphery. A summary of the prior work discussed in Section 1.2 is described in Table 1.1.

Table 1.1 Summary of Prior Work

Passini et al. [1]	Studied mechanisms of pro-arrhythmic abnormalities in ventricular repolarization in cases of hypertrophic cardiomyopathy
Ovchinnikova et al. [2]	Modeled cardiac hypertrophy by subjecting hESC-CMs to mechanical stretch to mimic molecular mechanisms and uncover biomarkers
Chang [5]	Used theoretical and experimental models to affect action potential propagation in cardiac tissue to better understand the electrogram
Ibrahim et al. [4]	Modeled cardiac electrical activity using bidomain and Fitzhugh-Nagumo models and varying ionic parameters
Bantle [7]	Modeled the electrical activity of a wedge of ventricular heart tissue by coupling the bidomain and Ten Tusscher models
Tanyous [6]	Mapped electrical propagation in the sinoatrial node using an in-silico model to validate an experimental model

1.3 Outline

It is important to bridge the gap between in vitro studies on ionic mechanisms of HCM and computational studies on general cardiac electrophysiology. Assessing cases of HCM through in silico studies will allow researchers to reach conclusions on the molecular activity of diseased cardiac tissue by altering various ionic mechanisms to pinpoint root causes and targeted areas of HCM. The objective of this thesis is to determine whether a three-dimensional computational model of cardiac tissue can mimic hypertrophic cardiomyopathy by varying the tissue thickness to observe changes in the shape of the action potential as it propagates through the tissue. Specifically, the analysis of the change in membrane potential in an action potential as it propagates through tissues of varying thickness will be useful to understand how a change in cardiac tissue thickness will impact the heart's ability to transmit an electrical impulse and therefore how likely it is for the heart to experience HCM. A three-dimensional computational model is not limited in the way that a clinical, animal, or in vitro study would be since it allows for the flexibility of parameter alteration and can accurately represent the mechanisms responsible for HCM in humans.

The organization of the paper is as follows: first, the background of the human cardiovascular system, the conduction of the electrical impulse of the heart, the cardiac action potential, membrane potential, hypertrophic cardiomyopathy, ventricular myocyte remodeling, and modeling cardiac tissue will be described; mathematical descriptions and the methods for the setup of the Beeler-Reuter and bidomain models in MATLAB will be outlined; the results of the analysis will be presented, validated, and statistically analyzed; and the results will be discussed as they pertain to the goal of this thesis. A statistical analysis will be performed in JMP, a suite of computer programs for statistical analysis that was developed by John Sall in the 1980's (JMP stands for "John's Macintosh Project"), to determine if a significant difference exists between the action potentials that stem from tissues with different thicknesses. The model will be validated by first visually comparing the output of the algorithm for membrane potential of a single ventricular myocyte, as described by the Beeler-Reuter model, to that which is found in the literature [9]. Once that algorithm has been validated, the active three-dimensional model will be compared to a

passive three-dimensional model to determine if the injected stimulus current has a noticeable effect. The accuracy of the electrical components' representation of the physiological components will be validated by describing the role of gap junctions, how they are affected during hypertrophic cardiomyopathy, and how their electrical equivalents predispose a prolonged action potential during cases of hypertrophy. Clinical data such as human cardiac action potential dynamics are scarce or limited in the literature by practical or ethical concerns [10]. Thus, such data was unable to be obtained for validation purposes in this paper.

This study seeks to answer whether the presented three-dimensional computational model can depict changes in the shape of an action potential moving through cardiac tissue of varying thickness. The purpose of this investigation is to see if the resulting action potentials will mimic those seen in cases of hypertrophic cardiomyopathy. The shape of the action potential is hypothesized to elongate in phases two and three with an increase in tissue thickness.

Chapter 2

BACKGROUND

2.1 The Human Cardiovascular System

The function of the heart is to pump oxygenated blood to all tissues within the body and to pump deoxygenated blood to the lungs. The heart consists of four chambers: the left and right atria and the left and right ventricles. The upper chambers, or the atria, receive blood coming from the systemic and pulmonary systems. They push blood into the lower chambers, or the ventricles, to be ejected to the lungs and the rest of the body. The atria are separated by the interatrial septum and the ventricles are separated by the interventricular septum. The septum between the atria and ventricles is known as the atrioventricular septum, marked by four valves that allow blood to flow from the atria to the ventricles [11]. Each of the major pumping chambers of the heart ejects approximately 70 mL of blood per contraction in a resting adult. The shape and size of the heart can be thought of as an inverted pear. It sits within the thoracic cavity and is medially located between the lungs. The superior and inferior vena cavae, the aorta, and the pulmonary trunk are located on the superior surface of the heart, known as the base. The inferior surface of the heart, known as the apex, lies to the left of the sternum. Figure 2.1 depicts the structural arrangement of the components described above within the heart.

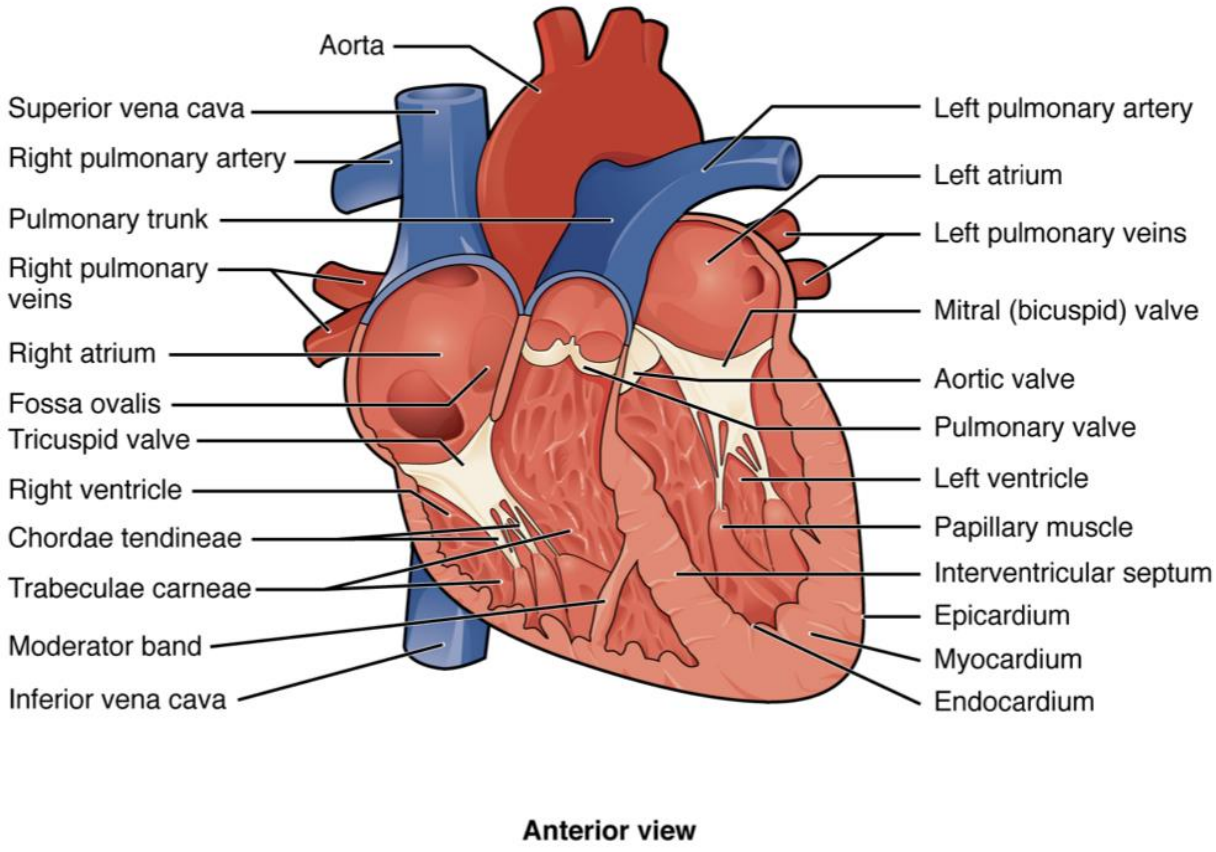

Figure 2.1. The anatomical structure of the human heart [11].

The size of the average adult's heart can be compared to a clenched fist. However, the heart of a well-trained athlete can be considerably larger than normal. Similar to skeletal muscle, cardiac muscle increases in protein myofilaments as a result of exercise, increasing the size of individual cells.This is known as physiological hypertrophy. The heart remodels itself in response to an increase in exercise to pump blood more effectively throughout the body. In the average adult heart (whether they are physically active or not), the left ventricle is considerably larger than the right ventricle. It is thicker and more developed so that it can overcome high resistance and develop a large amount of pressure required to pump blood into the long systemic circuit. The right ventricle does not require as much pressure to overcome resistance because the pulmonary circuit is much shorter than the systemic circuit and therefore has much less resistance [11].

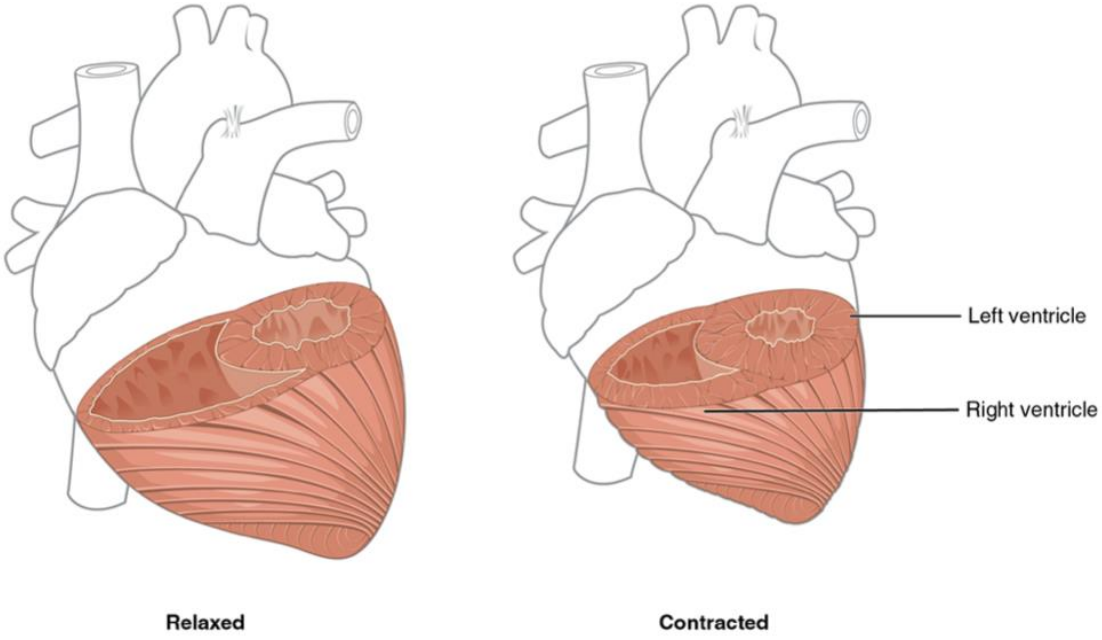

Figure 2.2. Differences in ventricular muscle thickness of a healthy human heart [11].

There are two distinct but linked circuits within the cardiovascular system: the pulmonary and systemic systems. The pulmonary circuit transports blood to and from the lungs, where it picks up oxygen from inhalation and delivers carbon dioxide for exhalation. The systemic circuit transports oxygenated blood to almost all tissues within the body (excluding the lungs) and returns deoxygenated blood and carbon dioxide to the heart to be sent to the lungs for the carbon dioxide to be exhaled and for the deoxygenated blood to be reoxygenated. Highly oxygenated blood returns to the heart through the pulmonary veins. They conduct blood into the left atrium, which pumps blood into the left ventricle, sending blood out to the systemic circuit. Deoxygenated blood flows into the superior and inferior vena cavae, returning blood to the right atrium. The right atrium then pumps blood into the right ventricle which sends blood into the pulmonary circuit to expel waste and to be reoxygenated [11].

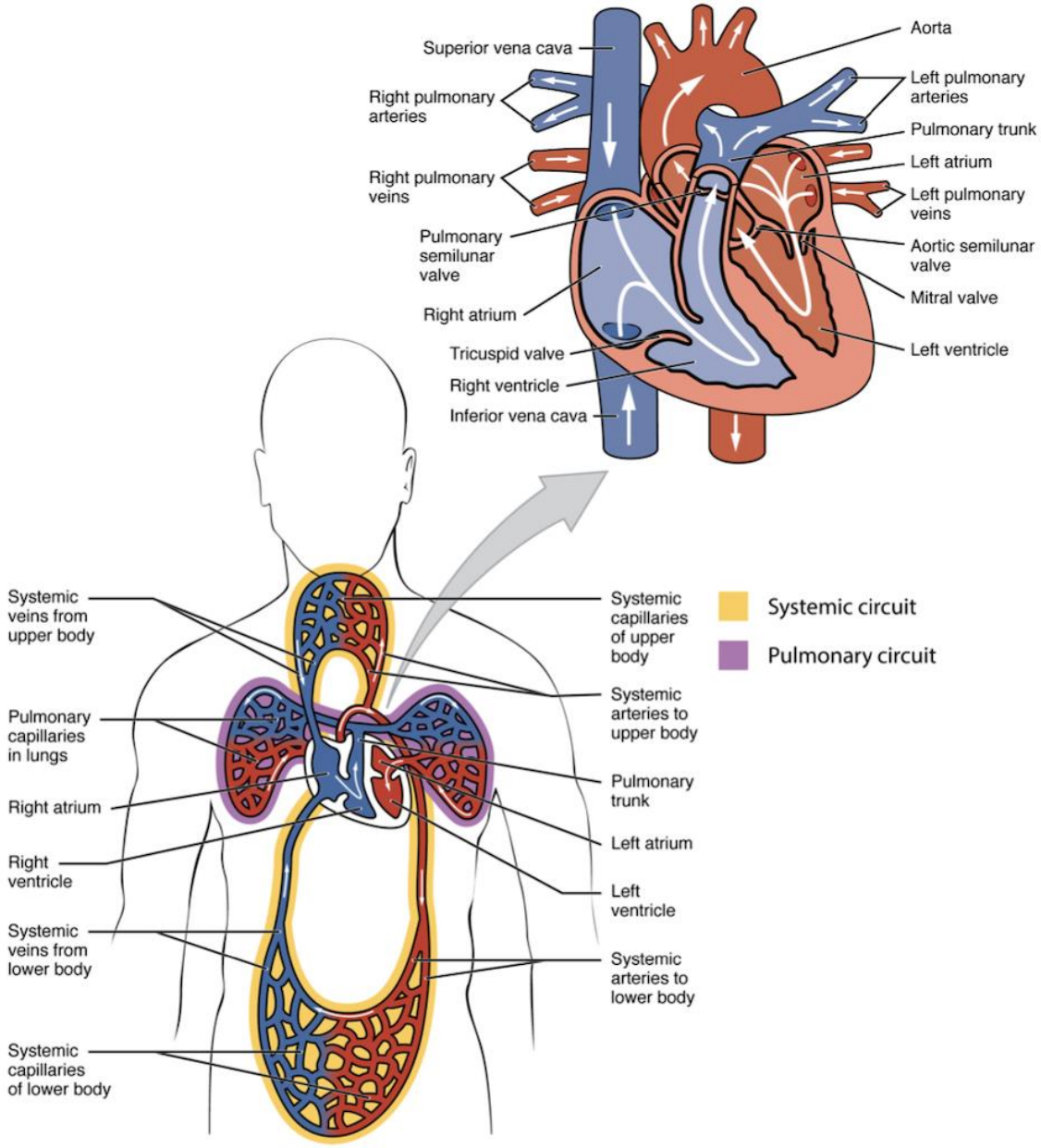

Figure 2.3. The dual system of human blood circulation: the systemic and pulmonary circuits [11].

2.2 Conduction System

The conduction system of the heart is arranged to allow for spontaneous firing and rapid transmission of an electrical impulse throughout the entire heart. It controls the timing of the electrical transfer between the atria and the ventricles, allowing for optimum hemodynamic performance [12]. Two key structural components of cardiac tissue that enable rapid, synchronous impulse transmission are intercalated disks and gap junctions. Intercalated disks mechanically connect adjacent cardiomyocytes while gap junctions electrically connect them. Gap junctions are structured as rings made up of proteins called connexons. They allow ions, nutrients, metabolites, and small proteins to pass. But most importantly, gap junctions allow the transfer of electrical impulses from one myocyte to the next.

The primary electrical components of the conduction system include the sinoatrial (SA) node, the atrioventricular (AV) node, the bundle of His, the left and right bundle branches, and the Purkinje fibers. The sinoatrial node is found at the top of the right atrium (near the entrance to the superior vena cava); the atrioventricular node is found at the interatrial septum; the bundle of His extends down from the atrioventricular node into the septum; the bundle branches disperse into their respective ventricles; and the Purkinje fibers are extensions of each set of bundle branches into the ventricular walls [12].

Pacemaker cells in the sinoatrial node spontaneously depolarize, dispersing an electrical impulse throughout both atria allowing them to contract simultaneously. The depolarization spreads from the right atrium to the left atrium through Bachmann's bundle [13]. The impulse then travels from the sinoatrial node to the atrioventricular node through the internodal fibers. Once the electrical impulse reaches the atrioventricular node, there is a slight delay in transmission to allow the ventricles to fill. Cells in the AV node conduct slower than those in the SA node to allow this delay in the electrical impulse transmission from the atria to the ventricles [12].

Once the ventricles are sufficiently filled, the electrical impulse rapidly travels down the bundle of His into the left and right bundle branches and finally to the Purkinje fibers located in the walls of the ventricles. The rapid conduction velocity of the latter half of the conduction system can be attributed to larger cell sizes, a unique distribution of gap junctions along the cell borders,

and an encapsulating fibrous sheath surrounding the conduction network [12]. Figure 2.4 portrays the conduction system embedded within the structure of the heart.

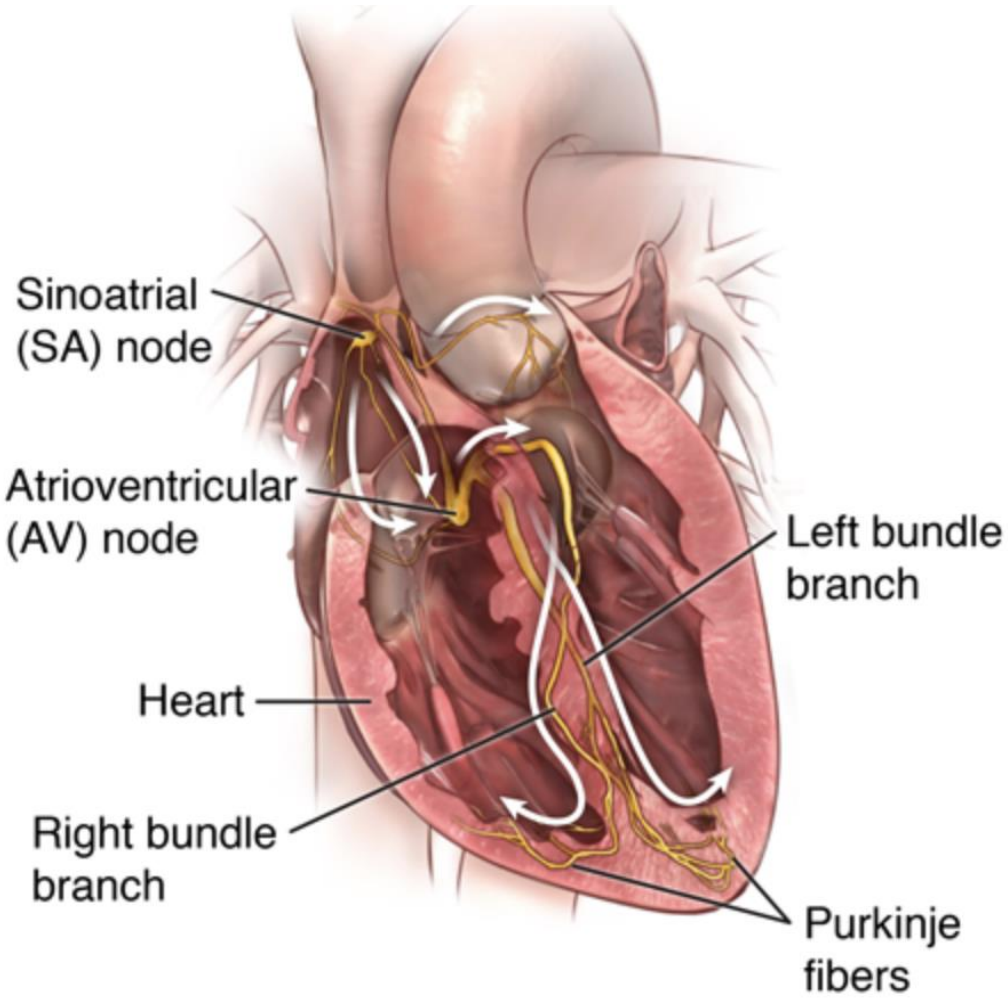

Figure 2.4. Electrical conduction system of the human heart [14].

2.3 Cardiac Action Potential

An action potential is the transmission of an electrical impulse which is the result of a rapid sequence of changes in the membrane potential. In an adult mammalian heart, the cardiac action potential travels as an electrical impulse through the heart's conduction system as a

means for maintaining the regular contractions of the heart to maintain perfusion to vital organs within the body [13]. During each heartbeat, the signal to contract reaches cardiac muscle cells in the form of an electrical impulse. At the cellular level, this electrical impulse causes a rapid release of calcium ions from intracellular stores to activate contraction in the sarcomere. This sequence of events from electrical excitation to force production is known as cardiac excitation-contraction coupling. Ion channels and their accessory proteins at the cell membrane are responsible for detecting and propagating the transient changes in the membrane potential that initiate contraction. Electrical changes in the membrane potential open L-type Ca^{2+} channels, triggering Ca^{2+} release from the sarcoplasmic reticulum in a process known as Ca^{2+}-induced release. Membrane-bound proteins in the sarcoplasmic reticulum are responsible for Ca^{2+} reuptake from the cytosol, which lowers Ca^{2+} and causes its contraction to end [15]. It could be perceived that the entire process of force generation by the myofilaments forms part of the excitation-contraction coupling. This sequence of events proves that an understanding of the relationship between excitation and the force produced by contraction depends critically on the properties of myofilaments.

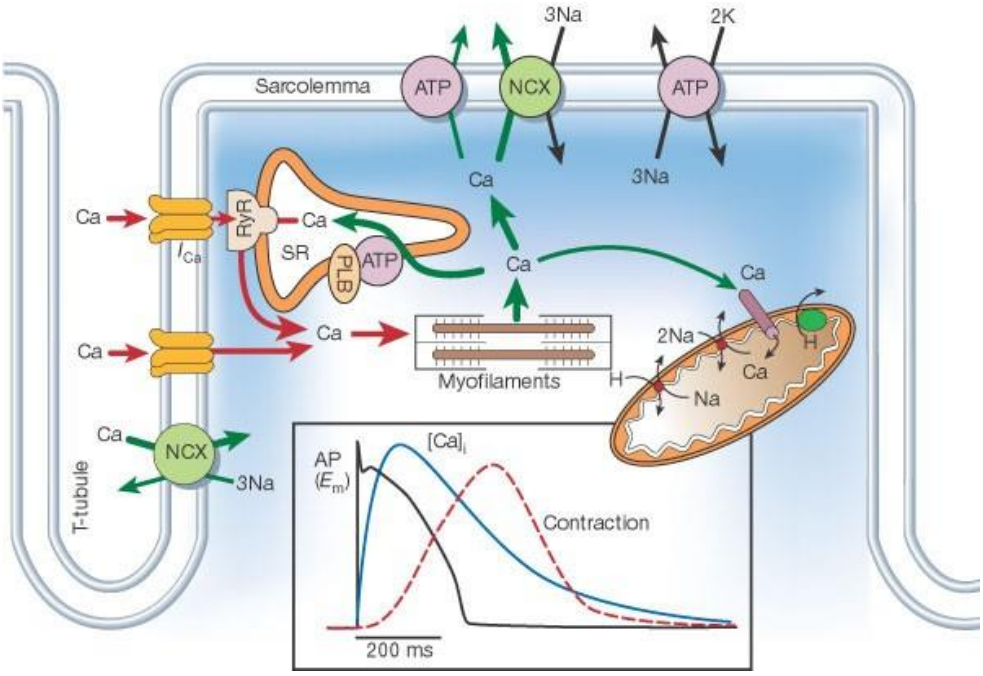

Figure 2.5. Excitation-contraction coupling in cardiac muscle [16].

The cardiac action potential differs from those that propagate through the nervous system for two main reasons: automaticity and a delayed plateau phase. Automaticity is only found in pacemaker cells within the heart because they have the intrinsic ability to depolarize rhythmically and initiate an action potential. The delayed plateau phase, while only found in the action potentials of cardiomyocytes, serves to allow enough time for muscle contraction during Phase 2 of the action potential.

There are a total of five types of cells that make up the adult mammalian heart: cardiomyocytes cells, pacemaker cells, fibroblasts, endothelial cells, and perivascular cells. Cardiomyocytes and pacemaker cells are the most abundant and the most crucial for propagating action potentials. Cardiomyocyte cells and pacemaker cells elicit different action potential waveforms. In this paper, the cardiomyocyte cell action potential is highlighted and discussed as it pertains to the Beeler-Reuter model of ventricular cardiomyocytes.

There are five phases to the cardiomyocyte action potential. A depiction of these five phases can be seen in Figure 2.5. They are structured in the sequence as follows:

- *Phase 0*: During this phase, rapid depolarization takes place. Voltage-gated sodium channels open causing an influx of sodium ions which brings the membrane potential to +50 mV. This accounts for the steep upstroke in the shape of the action potential
- *Phase 1*: During this phase, there is a slight drop in the membrane electrochemical potential. The previously open sodium channels inactivate while potassium channels activate a transient outward potassium current
- *Phase 2*: This is considered as the ‘plateau’ phase. There is a calcium ion influx, balancing the potassium ion efflux – this creates a plateau around +50 mV. Subsequently, the calcium ion influx stimulates the calcium release from the sarcoplasmic reticulum, initiating muscle contraction.
- *Phase 3*: Repolarization takes place. Calcium ion channels close and there is a continued potassium ion efflux through the opening of rapid delayed rectifier potassium channels.

- *Phase 4*: The repolarizing current from Phase 3 brings the membrane potential back to its initial resting value and is maintained by a potassium current.

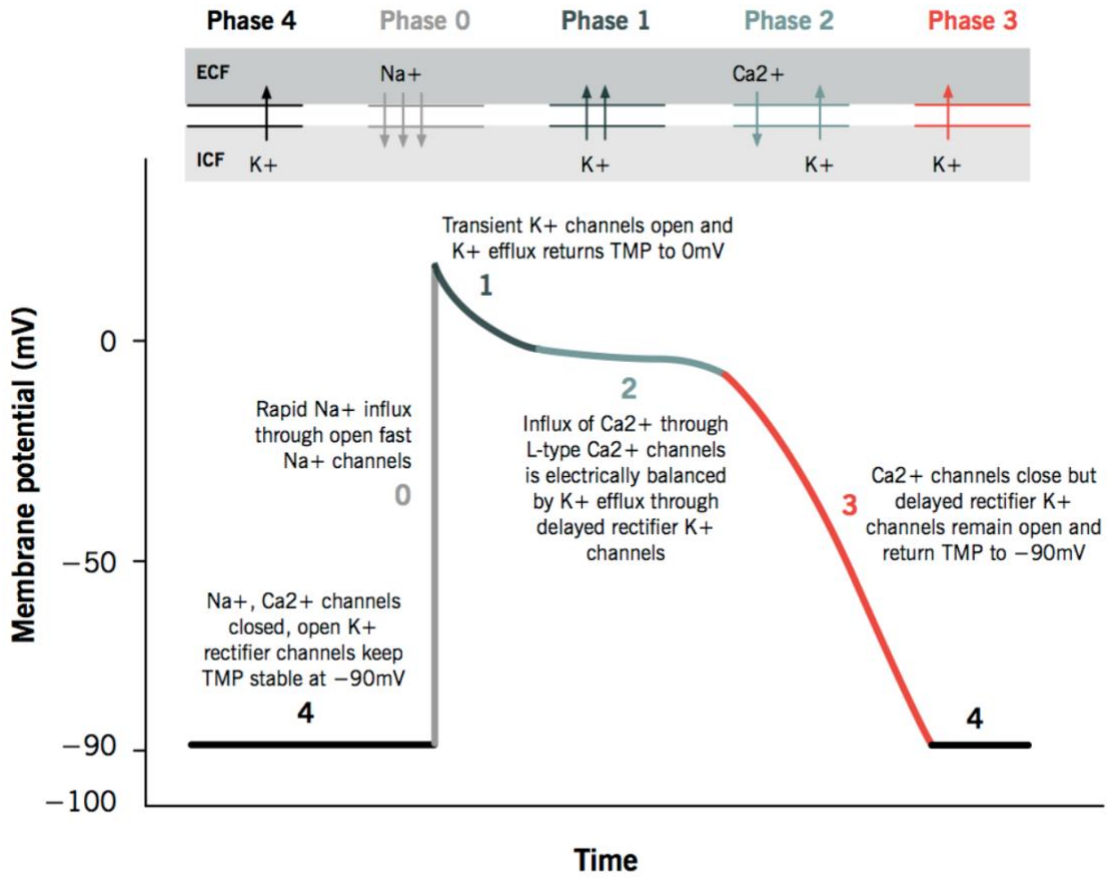

Figure 2.6. Phases of the cardiac action potential [15].

2.4 Membrane Potential

Membrane potential is a phenomenon that facilitates the propagation of an action potential in excitable tissues [16]. It will always remain in either a resting or active state. The resting membrane potential is maintained by the cells' ion channels [16]. In the resting state, the cell membrane maintains an equilibrium potential (which can be determined by the Nernst equation). The resting state of the cell membrane is determined primarily by two factors: the differences in ion concentration of both the intracellular and extracellular fluids, and the relative

permeabilities of the plasma membrane to different ion species. The cell membrane is a lipoprotein complex (7-15 nm thick), and during the resting state is only slightly permeable to sodium ions and freely permeable to potassium ions. Essentially, the cell membrane can be described as a leaky capacitor. The potassium concentration difference between the inside and outside of the cell creates a diffusion gradient for potassium ions to flow outwards, making the cell interior more negative. However, the electric field supported by the membrane at rest tends to inhibit the outward flow of positively charged ions (e.g., K+) as well as the inward flow of negative ions (e.g., Cl-). This makes the diffusional and electrical forces acting across the membrane opposed to each other, creating an equilibrium potential [17]. The resting membrane potential becomes active when an adequate stimulus influences the ionic concentration in the cell, initiating a depolarization.

Emerging evidence shows that a dynamic membrane potential is essential for many other processes including cell cycle, cell volume control, proliferation, and muscle contraction (even in the absence of an action potential). The maintenance of cell volume in particular is essential for cell survival, and membrane potential is a key regulator of this in cardiomyocytes. The membrane potential feeds into the cell volume control mechanism by changing the driving force for ionic current fluxes [16]. Since changes in cell volume are accompanied by ionic current fluxes, the change in cell volume may influence membrane excitability, contraction, and cellular homeostasis [18]. While it was formerly believed that cardiac tissue hypertrophy was the result of cardiomyocyte proliferation, recent studies have found that adult cardiomyocytes grow through hypertrophy (increase in cell size) instead of hyperplasia (increase in cell number). Cardiac cells proliferate as embryos, but that proliferation turns into cell hypertrophy as the cardiac cells mature [19]. Since it is known that membrane potential is a key regulator of cardiomyocyte cell volume, it is understandable why hypertrophic cardiomyopathy alters the shape of the action potential as it propagates through the cell membrane.

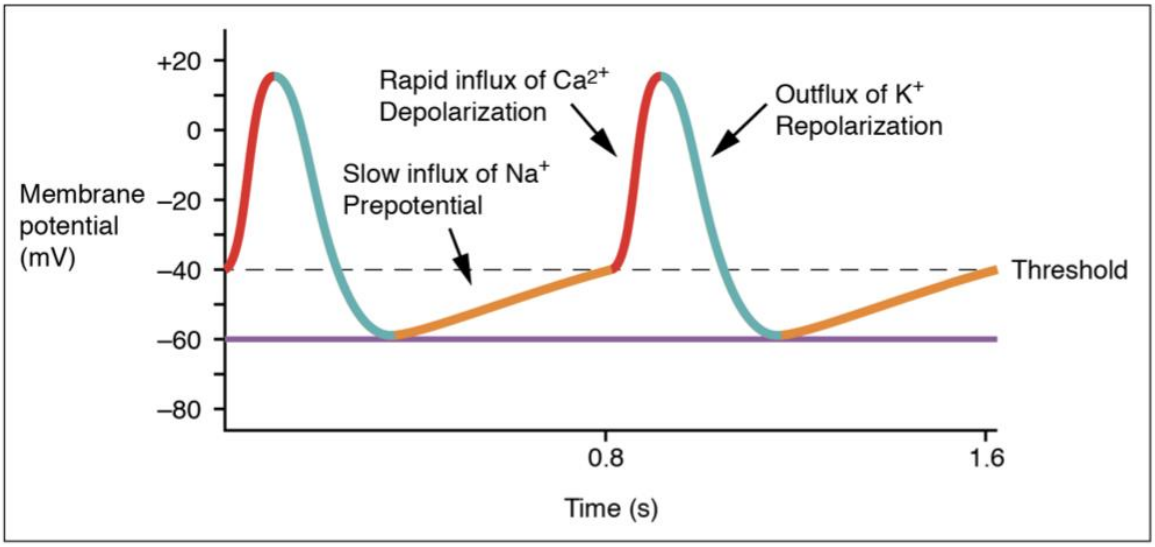

Figure 2.7. Fluctuation in membrane potential in cardiac cells during an action potential [11].

2.5 Hypertrophic Cardiomyopathy

Unexplained hypertrophic cardiomyopathy (HCM) is present in one out of every 500 adults in the United States [15]. HCM is the default diagnosis for patients presenting with left ventricular wall thickness, but without causative factors such as hypertension. It can be most simply defined as the increase in cardiac tissue size to compensate for a reduction in cardiac function. This compensation activates the sympathetic nervous system, the renin-angiotensin-aldosterone systems, and other neurohormonal mechanisms. The activation alters signal transduction, leading to a change in gene expression that produces myocyte hypertrophy [20]. In the majority of cases, HCM can be traced to genetic factors. Genetic linkage studies, the first appearing two decades ago, have identified mutations to sarcomeres as the primary cause. The inherited form of the disease, familial hypertrophic cardiomyopathy (FHC), is associated with left ventricular wall thickness, myocardial fibrosis, myocyte disarray, and increased risk of sudden cardiac death. The implicit hypothesis in current FHC research is that hypertrophy, regardless of its advanced form, is the result of altered acute function at the level of the cardiac sarcomere [15]. HCM is often asymptomatic and first presents itself during instances of cardiac failure, particularly

ventricular tachyarrhythmias. It is the most common monogenic disorder and is the main source of sudden cardiac death in children and young adults [1]. The intrinsic cardiac and peripheral responses to myocardial failure adversely alter the electrophysiology of the heart, predisposing patients with heart failure to an increase in arrhythmic death [20]. No cure exists for the condition, and treatments to alleviate the symptoms are limited.

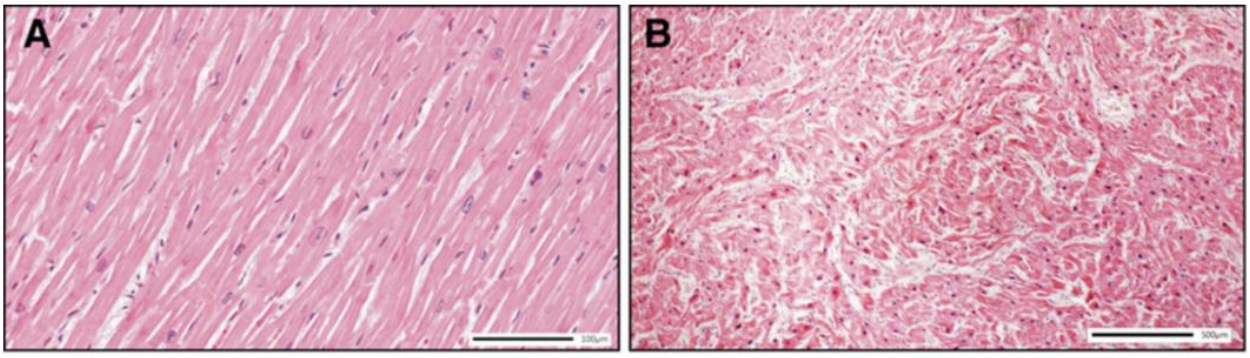

Figure 2.8. (A) A normal thin myocardial section stained with H&E. (B) A low magnification (×4) H&E-stained thin myocardial section from a patient heart with HCM [8].

There is evidence in the literature [1, 20, 21] that a consequence of hypertrophic cardiomyopathy is a prolonged repolarization period in the action potential of cardiomyocytes as well as a prolonged presence of calcium transient current. Passini et al. found that L-type calcium current reactivation contributed to repolarization abnormalities in cardiomyocytes. Coltart et al. described how previous investigations into prolonged repolarization of cardiomyocytes attributed that abnormality to reasons such as massive, short irregular fibers with abnormal nuclei, a subset of other cardiac diseases, and having excessive noradrenaline deposits in the diseased muscle. However, this study found that hypocalcemia was a contributing factor to prolonged repolarization periods in cardiomyocytes. Tomaselli et al. discussed the implications of functional alterations in the depolarizing and repolarizing currents as the general reason for changes in the action potential during HCM. Specifically, the down regulation of potassium currents was highlighted as a recurring theme in hypertrophied myocardium and additionally how a fluctuation in L-type calcium current density typically precedes cardiac hypertrophy.

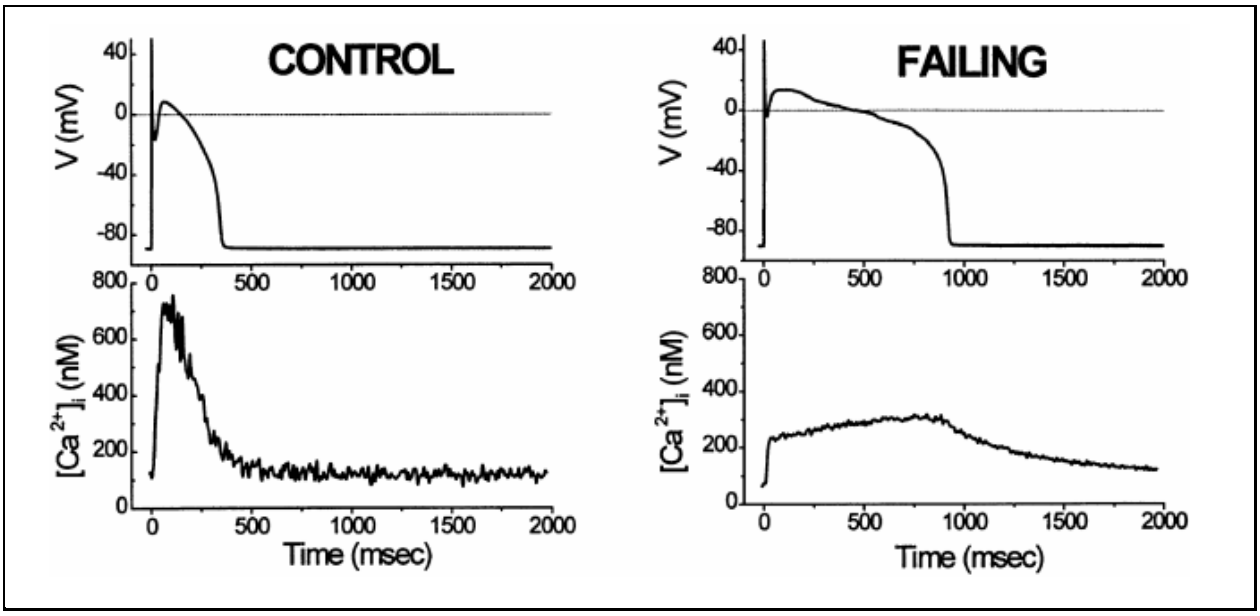

Figure 2.9. Transmembrane potential (top) and transient calcium current (bottom) in healthy (left) and failing (right) cardiomyocytes [20].

From Figure 2.9, there is evidence of a distinction between the repolarization duration of healthy cardiomyocytes versus diseased cardiomyocytes. The longer the action potential duration, the more the repolarization process is subject to change. With a change in the shape of the action potential comes electrical remodeling of the cardiac tissue. The stage of disease is crucial in determining the degree and character of electrical remodeling and arrhythmic risk [20]. Abnormal automaticity may arise in hypertrophied cardiac tissue in the setting of a reduction in resting membrane potential. In fact, the most common mechanism of ventricular arrhythmias is reentry due to abnormal impulse conduction. Such an abnormal conduction rate may contribute to the production of arrhythmias in hypertrophic and failing hearts [20].

The key components of ventricular myocyte remodeling are the functional expression of a number of ion channels, transporters and receptors that result in action potential prolongation, and abnormal Ca^{2+} handling and aberrant adrenergic signaling. The great challenge that remains is to use insight provided by in vitro studies to better understand these components of ventricular myocyte remodeling and how they contribute to arrhythmic mechanisms so that sudden death may be prevented in patients [20].

2.6 Ventricular Myocyte Remodeling

Structural remodeling in ventricular myocytes is a major feature of cardiac hypertrophy and of heart failure. An understanding of the abnormal signaling underlying the associated cellular changes should have considerable clinical benefits. It is known that myocyte transverse growth (as opposed to longitudinal growth) is largely responsible for wall thickening during cardiac hypertrophy [24]. The increase in chamber diameter provides the structural basis for the elevated wall stress found in heart failure, which can be preceded by hypertrophy. Due to the spatial arrangement of myocytes within the ventricular wall, cell diameter is primarily responsible for changes in wall thickness. The myocyte shape alterations during cardiac hypertrophy go hand-in-hand with changes in ventricular anatomy. Such shape alterations are a result of volume overloading, leading to proportional growth in the ventricular diameter and is reflected at the cellular level by the proportional growth of myocyte length and cross-sectional area [24].

There are distinct cellular and molecular events that occur between cardiomyocytes and non-cardiomyocytes that partially dictate the extent of remodeling in the cardiac tissue from volume overload. Cardiomyocytes have been proven to show phenotypic modification that results in cellular hypertrophy accompanied by reexpression of several fetal genes, abnormal Ca^{2+} handling, oxidative stress, and mitochondrial DNA damage and cardiomyocyte death due to necrosis or apoptosis. Cardiac fibrosis, or an excessive deposition of the extracellular matrix proteins, is a hallmark of pathological hypertrophy and heart failure [25]. By forming a barrier between cardiomyocytes, fibrosis can impair the electrical coupling of cardiomyocytes, leading to cardiac systolic dysfunction. Resident cardiac fibroblasts, the primary cells that contribute to fibrosis, are thought to arise from the embryonic proepicardial organ. During fetal development, their role is to proliferate and grow in size to help the heart to grow. These fetal genes become less prominent after sufficient fetal development. The cardiomyocyte-specific deletion of genes has been shown to affect not only cardiomyocyte functionality but also the phenotypes and functions of fibroblasts [26]. Conversely, recent studies have shown that cardiac fibroblasts control cardiomyocyte proliferation in the developing ventricles during embryogenesis and that

fibroblasts promote cardiomyocyte hypertrophy through paracrine factors and ECM. Many growth factors and cytokines have been shown to act in an autocrine or paracrine fashion to induce hypertrophic responses in cardiomyocytes and activate fibroblasts. Figure 2.10 shows the relationship between fibroblasts and myocyte hypertrophy with only some of the contributing factors identified.

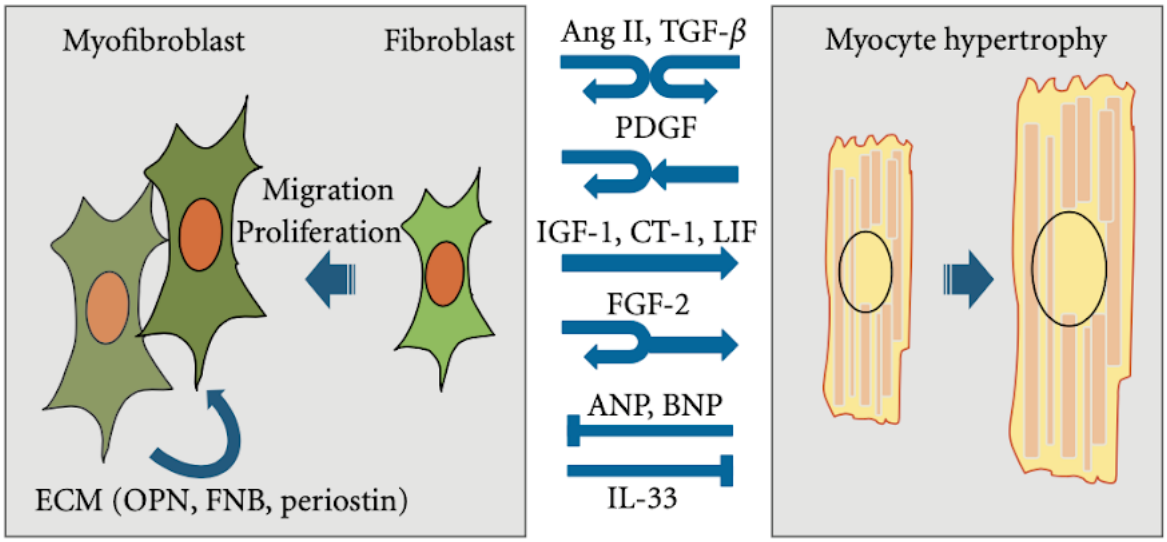

Figure 2.10. Reciprocal interactions between fibroblasts and cardiomyocytes [26].

Insulin-Like Growth Factor-1 (IGF-1) exerts adaptive and cardioprotective effects in response to stress. In the heart, IGF-1 is mainly expressed in cardiac fibroblasts and activates downstream signal transducers, such as phosphoinositide 3-kinase (PI3K), leading to cardiomyocyte hypertrophy. Additionally, cardiac IGF-1 is transactivated by KLF5, which controls IGF-1 expression in cardiac fibroblasts in response to stress [26]. This induction of IGF-1 is an essential cardioprotective response. It is theorized that the exacerbation of these factors contributes to the incitement of pathological hypertrophic cardiomyopathy.

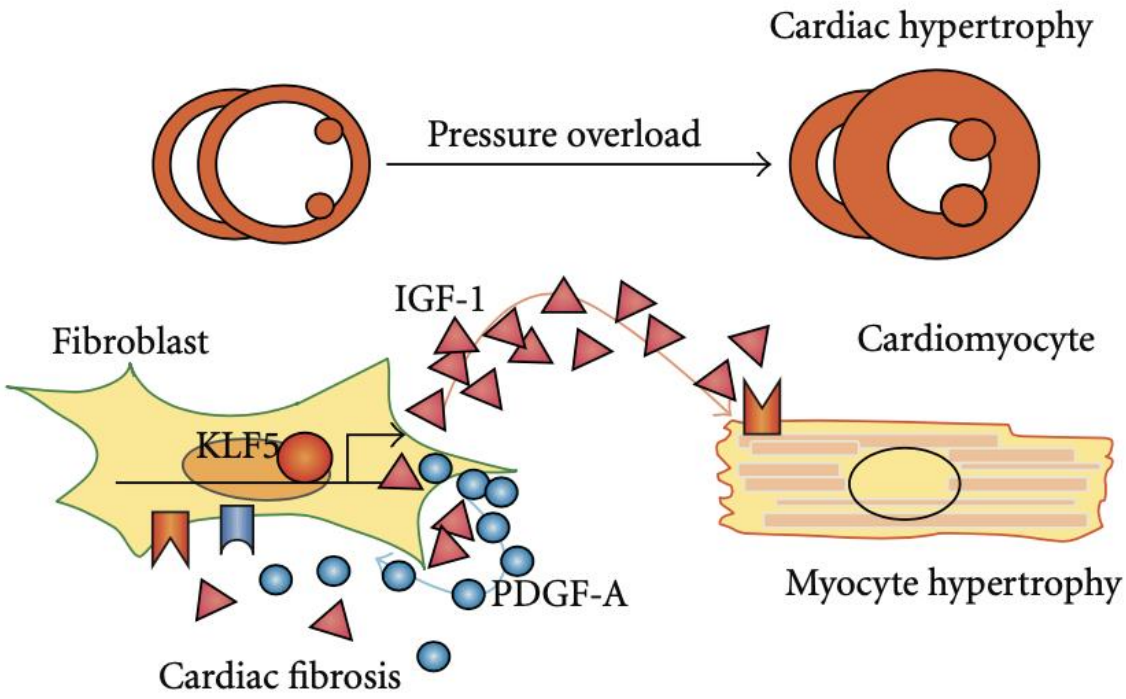

Figure 2.11. A model for the regulation of fibroblasts by KLF5 during cardiac hypertrophy [26].

2.7 Computationally Modeling Cardiac Tissue

Computational models of ventricular myocyte electrophysiology have evolved over several decades and have improved the biophysical accuracy and computational efficiency of modeling electrical dynamics through innovative mathematical approaches. The recent advances in computational modeling have revolutionized patient diagnostics and treatment by enabling the construction of three-dimensional models of cardiac tissue that are patient specific. It can be used to make inferences about biophysical phenomena that are difficult to investigate and cannot be readily measured. For example, it is challenging to investigate the molecular causes and structural mechanisms that underlie reentrant arrhythmias, such as tachycardia and fibrillation [12]. Computational models give researchers the power to manipulate certain biophysical parameters, providing the advantage of understanding the cellular mechanisms that dictate electrical and mechanical behaviors.

Computational models that are patient-specific optimize diagnostic treatment because they reveal information that would have otherwise been concealed. Using physiology and physics rather than population statistics to build such models has uncovered more interindividual variability in pathophysiology, indicating that patient groups are less uniform than previously thought. The inherent need for individualized treatment for cardiac diseases is rising. With the increase in computational power and tissue model complexity, simulations are becoming better able to provide the link between the effects of genetic mutations, physiological regulations or drugs on protein function and emergent cellular and tissue function or clinical phenotypes.

Three-dimensional (3D) tissue models that incorporate detailed structural information can provide details about the local electrical behavior that would not be otherwise available. However, 3D models typically assume a continuum and require meshes to be on the order of 100 million nodes to represent a full human heart. Time steps are required to be on the order of 0.01 seconds to achieve temporal convergence because the upstroke of the cardiac action potential is very rapid. This makes it challenging to use complex models to study rhythm disturbances where it is necessary to simulate several cycles of activation [12]. Over recent years, computational power has increased, allowing for finer meshes and more complex current models to be used in modeling cardiac tissue. As this power continues to increase in the future, it will become easier to obtain the most realistic in-silico model of an entire human heart.

To satisfy tissue electrodynamics, cellular-level models can be incorporated into larger-scale models as a discrete set of cells or tissues, assuming that at each node point there exists both intracellular and extracellular space. The fundamental relationships for a three-dimensional electrical continuum are described below [12].

$$E = -\nabla\phi \tag{2.1}$$

where E is the electric field (with units of Newtons per Coulomb, N/C) and φ is the potential (with units of Volts, V).

$$J = \sigma E \tag{2.2}$$

where J is current density (with units of milliampere per square meter, mA/m^2) and σ is the conductivity of the medium (with units of Siemens per meter, S/m).

$$\nabla J = I_v \tag{2.3}$$

where I_v is the source density (with units of ampere per meter A/m).

$$\nabla^2 \phi = -I_v \sigma \tag{2.4}$$

otherwise known as Poisson's equation.

Chapter 3

METHODS

The Beeler Reuter model was combined with the bidomain model to simulate the electrical dynamics of a ventricular myocyte for the purpose of investigating the effects of hypertrophic cardiomyopathy (HCM) on the related action potential dynamics. The bidomain model was designed to be a three-dimensional cable model, serving as a piece of cardiac tissue, with the Beeler Reuter model simulating the ionic current fluctuations at each node as an action potential propagates through the model. The piece of cardiac tissue was designed with a rectangular shape for simplicity. This simulation is useful for understanding how changes in ventricular tissue thickness impact electrical impulse propagation and the ventricles' overall ability to contract.

While more complex ionic current models have been developed in recent years, the Beeler Reuter model was selected for its ease of use solving a matrix in MATLAB. The bidomain model was selected as it is the most mathematically accurate model of electrical behavior within cardiac tissue and is relatively straightforward to implement. A one-way ANOVA test was run to examine if there was a significant difference between the action potentials that resulted from pieces of tissue with different thicknesses

3.1 Beeler Reuter Model

The Beeler-Reuter model was developed in 1977 as an advancement of the Hodgkin-Huxley model. The formulation of differential equations for the time- and voltage-dependence of the activation parameters behaves identically to those of the first approach in the Hodgkin-Huxley model, only here the sodium gates activate and inactive. The Beeler-Reuter model can provide information on cardiac arrhythmias and ion transport in cardiac cells [9]. This model was selected for its simplicity and low computational requirements.

The Beeler-Reuter model uses four different ionic currents to simulate the action potential waveform in mammalian ventricular myocardial cells. The four ionic currents consist of an initial

fast inward current carried primarily by sodium ions (I_{Na}); a secondary or slow inward current carried mainly by calcium ions (I_s); a time-activated outward current carried primarily by potassium ions (I_{x1}); and a time-independent outward current carried mainly by potassium ions (I_K). Figure 3.1 shows the four ionic currents and their respective direction in and out of the ventricular myocyte.

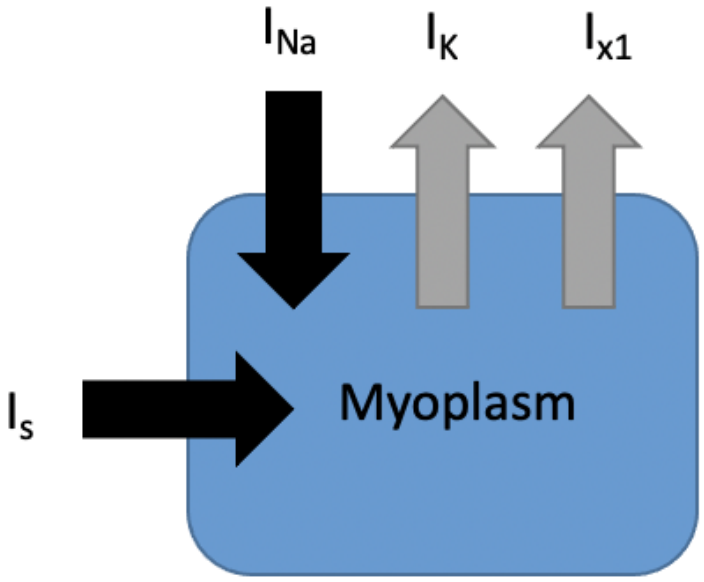

Figure 3.1. A schematic of the four ionic currents used in the Beeler Reuter model.

There are six conduction parameters that describe the degree of activation and inactivation of the ion-gated channels: *d*, a calcium activation gate; *f*, a calcium inactivation gate; *h*, a sodium inactivation gate; *j*, a second sodium inactivation gate; *m*, a sodium activation gate; and *x1*, a potassium activation gate. There are a total of eight parameters that serve as inputs to the model: the transmembrane potential V_m, the intracellular calcium concentration *Ca*, and the six conduction parameters that describe the degree of activation and inactivation of the ion gated channels *d*, *f*, *h*, *j*, *m*, and *x1*. The equations for each ionic current and the equation representing the overall ionic activity in the ventricular myocyte can be found in Figure 3.2. Values of calcium

dynamics, Nernst potentials, and conductance can be found in Table 3.1. Initial values of the state variables can be found in Table 3.2.

$$J_{ion} = J_{k_1} + J_{x_1} + J_{Na} + J_s \qquad \text{ion current through the membrane}$$

$$J_{k1} = 0.35\left\{\frac{4\{\exp[0.04(V_m+85)]-1\}}{\exp[0.08(V_m+53)]+\exp[0.04(V_m+53)]} + \frac{0.2(V_m+23)}{1-\exp[-0.04(V_m+23)]}\right\}$$

time-independent K^+ current

$$J_{x1} = x_1 \cdot 0.8\left\{\frac{\exp[0.04(V_m+77)]-1}{\exp[0.04(V_m+35)]}\right\} \qquad \text{time- and voltage-dependent } K^+ \text{ current}$$

$$J_{Na} = (G_{Na}\cdot m^3\cdot h\cdot j + G_{NaC})(V_m - E_{Na}) \qquad \text{fast } Na^+ \text{ current}$$

$$J_{Ca} = G_{Ca}\cdot d\cdot f\cdot(V_m - E_{Ca}) \qquad Ca^{2+} \text{ current}$$

Figure 3.2. Equations for ionic current activity in the Beeler-Reuter model [22].

Table 3.1. Values of Calcium Dynamics, Nernst Potentials, and Conductance

$\frac{d[Ca]_i}{dt}$	$-10^{-7}J_{Ca} + 0.07(-10^{-7} - [Ca]_i)$
E_{Na}	50
E_{Ca}	$-82.3 - 13.0287 * ln[Ca]_i$
G_{Na}	4
G_{NaC}	0.003
G_{Ca}	0.09

Table 3.2. Initial Values of State Variables

State Variable	Value	Dimensions
V_m	-84.62	mV
$[Ca]_i$	10^{-7}	mol/L
d	0.003	N/A
f	1	N/A
h	0.99	N/A
j	0.97	N/A
m	0.011	N/A
x1	0.0074	N/A

The action potential of a single ventricular myocyte, as described by the Beeler Reuter model, is represented in Figure 3.3. The code used to create the action potential can be found in Appendix A.

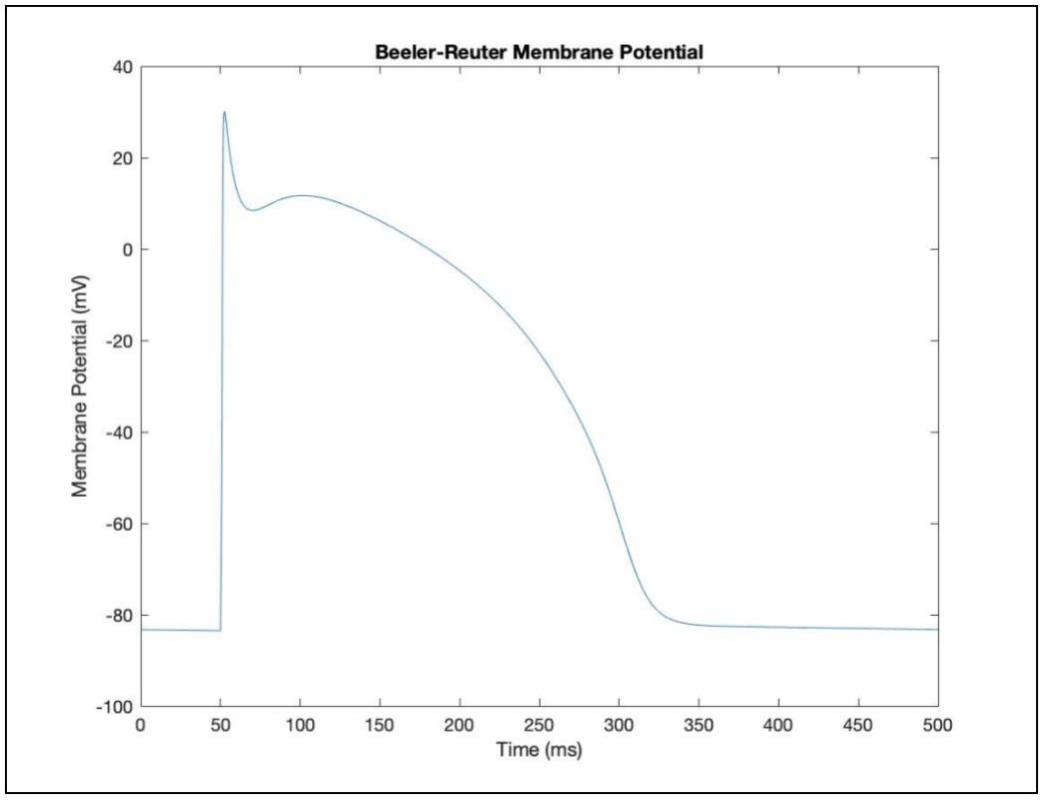

Figure 3.3. The action potential of the Beeler-Reuter model within a ventricular myocyte.

3.2 Bidomain Model

The bidomain model serves as the most complete representation of cardiac tissue. It is based on the assumption that, at the cell scale, the cardiac tissue can be partitioned into two ohmic conducting media, separated by the cell membrane: intracellular and extracellular domains [23]. It recognizes that cardiac tissue is electrically anisotropic and that, during electrical activation, current flows in both the extracellular and intracellular domains. Two of the most commonly measured cardiac electrical signals, extracellular potential and transmembrane potential, are direct model outputs [24].

The bidomain model was developed to be the first mathematical model that could describe the electrical properties of cardiac tissue which initially helped to unravel the mechanisms of how a pacemaker excites the heart. It represents cardiac tissue as a multidimensional cable that can be represented by a network of resistors and capacitors. For example, a two-dimensional bidomain model consists of one upper grid of resistors and one lower grid of resistors (i.e., the extracellular space and intracellular space, respectively) coupled by resistors and capacitors (i.e., the membrane) [24].

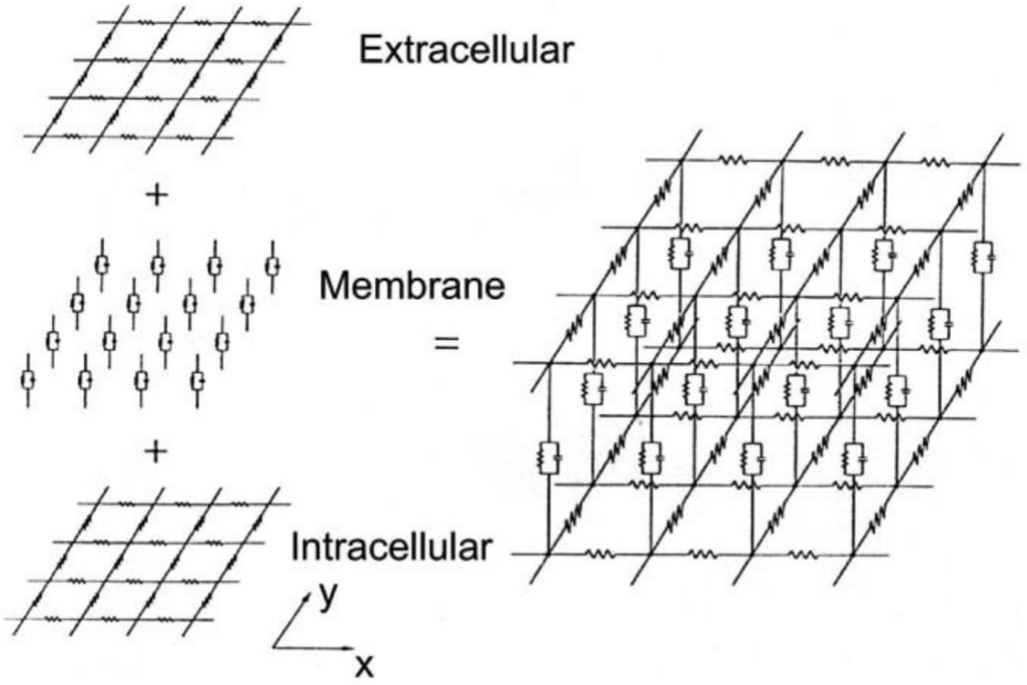

Figure 3.4. Two-dimensional bidomain network [29].

While Figure 3.4 represents a two-dimensional representation of myocardial tissue, a true working myocardium is regarded as a three-dimensional network of coupled excitable elements [27]. The resistor and capacitor in parallel are analogous to the gap junction between cardiomyocytes. Thus, the z-direction can be thought of as units of cardiomyocytes along with the intercalated discs that separate them. To perform appropriate simulations of cardiac electrophysiology, the bidomain model must be coupled with an ionic model to capture the full range of cell membrane kinetics [25]. An ionic model describes the chemical and electrical gradients across the cell membrane of a single cardiac cell by simulating the subcellular processes that take place within a selectively permeable membrane, which is permeable to different ions under different conditions [7].

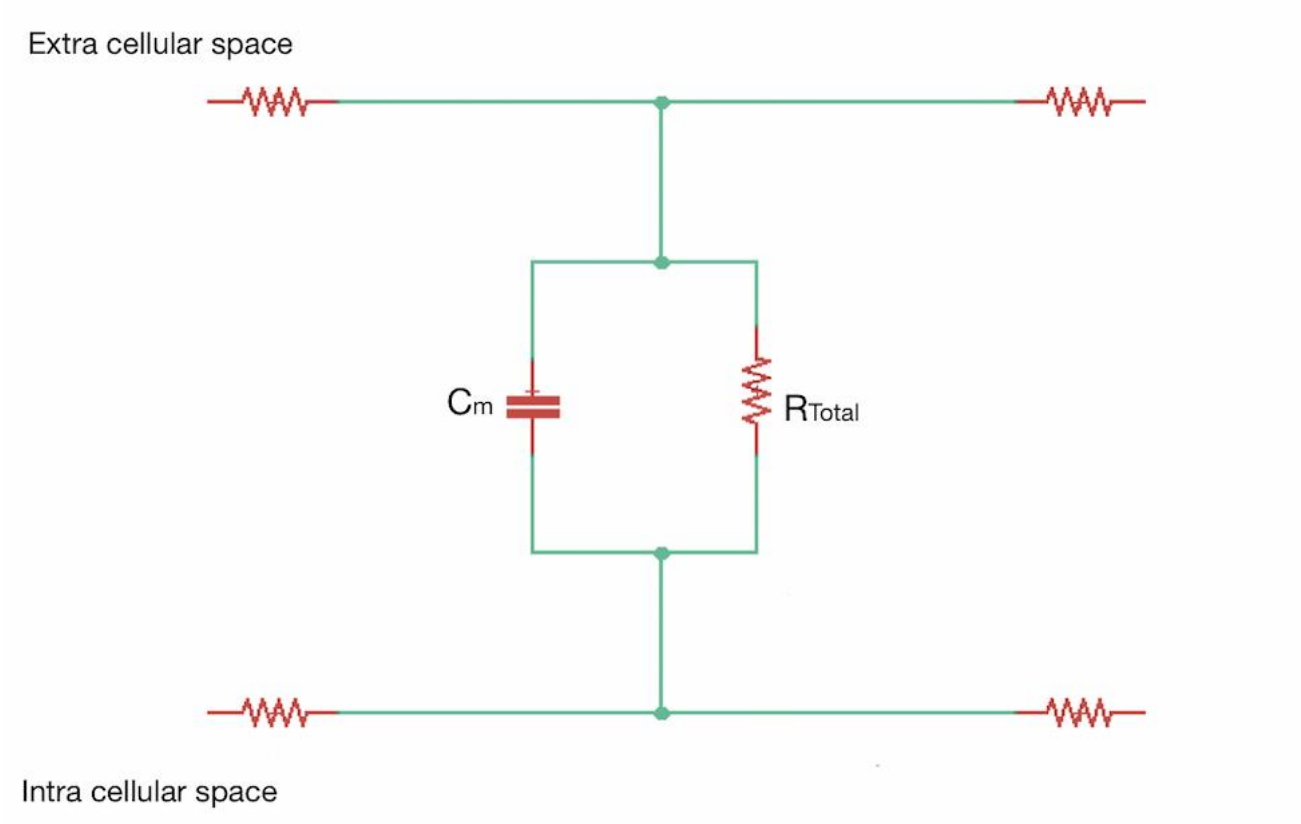

Figure 3.5. Ionic model represented by an equivalent circuit model.

The current flowing into the top center node from the capacitor and resistor in parallel in Figure 3.5 can be represented by the following equation:

$$C_m dV_m dt + I_{Na} + I_K + I_{x1} + I_s - I_{stim} = 0 \quad (3.1)$$

This equates to the right-hand side of the second bidomain equation (Eq. 3.8) described on page 34. The ionic currents used in Equation (3.1) represent the Beeler Reuter model. The one-dimensional equivalent circuit model in Figure 3.5 is the unit that is repeated in the multi-dimensional cable model shown in Figure 3.4.

Several ionic models are available with varying differential equations. The more complex models have been developed in recent years and are advancements on ionic models developed previously. Within cardiac tissue, changes occur rapidly over a small spatial domain, so discretized versions of these models must be solved on a fine computational grid and small-time

steps must be used. For very simple ionic models, the bidomain model can be discretized and numerical solutions can be computed for all variables simultaneously [25].

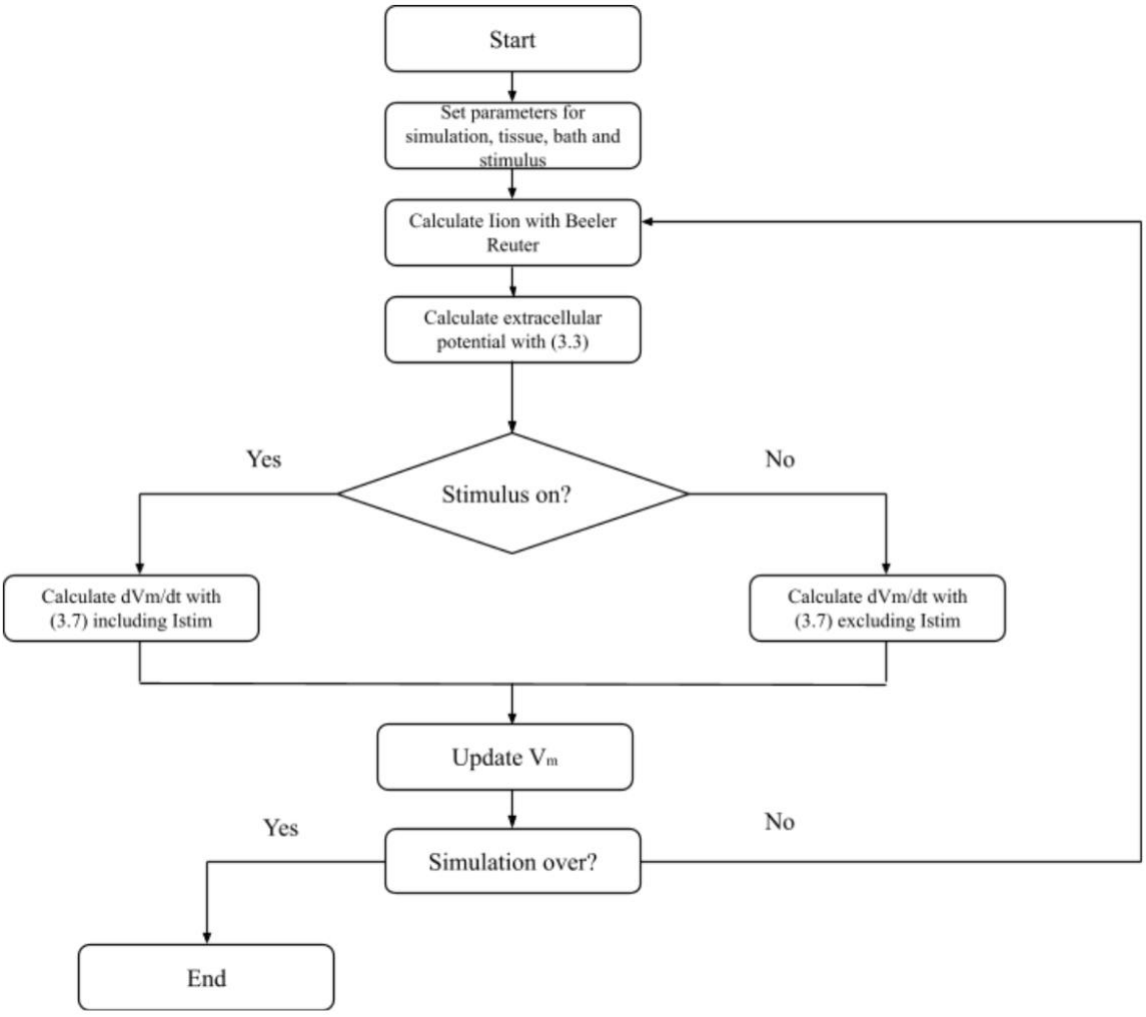

Figure 3.6. Flowchart of the steps taken to implement the bidomain model into MATLAB.

Table 3.3. Parameters Used in the Implementation of the Bidomain Model

Parameter	Description	Value
Δt	Size of time step	0.02 ms
h	Distance between node points	0.2E-3 m
σ_i, x	Intracellular conductivity in the x-direction	0.2 $\frac{S}{m}$
σ_i, y	Intracellular conductivity in the y-direction	0.02 $\frac{S}{m}$
σ_i, z	Intracellular conductivity in the z-direction	0.02 $\frac{S}{m}$
σ_e, x	Extracellular conductivity in the x-direction	0.2 $\frac{S}{m}$
σ_e, y	Extracellular conductivity in the y-direction	0.08 $\frac{S}{m}$
σ_e, z	Extracellular conductivity in the z-direction	0.08 $\frac{S}{m}$
σ_b	Conductivity of the surrounding bath	0.2 $\frac{S}{m}$
β	Surface area to volume ratio	3E5 $\frac{1}{m}$
C_m	Membrane capacitance per unit surface area	1 $\frac{F}{m^2}$
V_m, $t = 0$	Initial membrane potential	-83.3 mV
I_{Stim}	Stimulus current	3E5 $\frac{mA}{m^2}$

These values do not change within MATLAB model constructed in this thesis. The model was designed to be a continuum, wherein the electrical properties remain constant throughout the simulations. However, it is logical to assume that some of these values would change in a true case of hypertrophic cardiomyopathy. Given that cardiac disease does not progress uniformly, tissue conductivity may not be uniform throughout the tissue as it thickens. Additionally, the distance between node point (or reference points) will vary and be inconsistent by nature.

3.2.1 Mathematical Formulation of the Bidomain Equations

To define the mathematical formulation of the bidomain model, it is helpful to first start with the definition of transmembrane potential:

$$V_m = \phi_i - \phi_e \tag{3.2}$$

Here, ϕ_i represents intracellular potential and ϕ_e represents extracellular potential.

The basis of the bidomain model is that the net current flux between the intracellular and extracellular domains is zero everywhere and takes on the following form:

$$-\nabla \cdot J_i = \nabla \cdot J_e \tag{3.3}$$

By taking equations (2.1) and (2.2) and substituting them in for J_i and J_e, respectively, in equation (3.3), and by substituting in equation (3.2) for ϕ_i, the first bidomain equation is is written as:

$$\nabla \cdot (\sigma_i \nabla V_m) = -\nabla \cdot ((\phi_i + \phi_e)\nabla \phi_e) \tag{3.4}$$

Additionally,

$$-\nabla \cdot J_i = \beta I_m - I_s \tag{3.5}$$

where β is the surface-to-volume ratio, I_m is the transmembrane current density and I_s is an externally imposed current source density. From this expression, it can be shown that

$$\nabla \cdot (\sigma_i \nabla V_m) + \nabla \cdot (\sigma_i \nabla \phi_e) = \beta I_m - I_s \tag{3.6}$$

It's important to note that we define I_m as

$$I_m = C_m \frac{\delta V_m}{\delta t} + I_{ion} \tag{3.7}$$

where I_{ion} is the net current carried by the transmembrane ion channels. We combine equations (3.6) and (3.7) to get the second bidomain equation:

$$\nabla \cdot (\sigma_i \nabla V_m) + \nabla \cdot (\sigma_i \nabla \phi_e) = \beta \left(C_m \frac{\delta V_m}{\delta t} + I_{ion} \right) - I_s \tag{3.8}$$

3.2.2 Boundary Conditions of the Bidomain Equations

The boundary condition used for solving the bidomain equations is that there is no current flow out of the intracellular domain at the surface of the heart. This can be written as

$$(\sigma_i \nabla \phi_i) \cdot n = 0 \tag{3.9}$$

Where *n* is a unit vector outwardly normal to the myocardial surface. To match the formulation of the bidomain equations, this boundary condition can be further rewritten as

$$(\sigma_i \nabla V_m) \cdot n = -(\sigma_i \nabla \phi_e) \cdot n \tag{3.10}$$

3.2.3 Solving the Bidomain Equations

The bidomain equations must be both time discretized and spatially discretized. The time discretization will be solved using a forward Euler method and the spatial discretization will be solved using the finite difference method. The potential at each point in the tissue is a function of its neighboring points and can be represented through the following equation:

$$\nabla \cdot (\sigma \nabla \phi) = \sigma \nabla^2 \phi = \sigma_x \frac{\partial^2 \phi}{\partial x^2} + \sigma_y \frac{\partial^2 \phi}{\partial y^2} + \sigma_z \frac{\partial^2 \phi}{\partial z^2} \tag{3.11}$$

3.2.3.1 Time Discretization

The time discretization of the bidomain model will be solved using the forward Euler method. This method is a first-order numerical procedure for solving ordinary differential equations with a given initial value. It is the most basic explicit method for numerical integration of ordinary differential equations and was thus selected for its simplicity.

3.2.3.2 Spatial Discretization

The spatial discretization of the bidomain model will be solved using the finite-difference method in this paper. The finite-difference method, while not often used for irregular shaped geometries such as cardiac tissue, has a simple formulation, low computational requirements,

and is fast to solve [26]. The finite difference technique is well-suited for a discontinuous myocardial structure with no-flux boundaries. It approximates the solution of differential equations by using the finite differences of the neighboring node points [7]. This is implemented by a Laplacian matrix, described by the operator $\nabla^2\sigma$. Numerically, this technique is straightforward, but it requires a uniformly spaced solution grid. For a three-dimensional model, sufficient discretization requires a large quantity of node points, thereby increasing the computational requirements. To decrease computational time, the quantity of node points in each direction was restricted to ten nodes. A linear system of algebraic equations arises from the spatial discretization which will be solved with an iterative solver. An iterative solver was selected over a direct solver due to its efficiency in solving large matrices [7].

3.3 Simulating Electrical Activity in a 3D Model of Cardiac Tissue

The geometry of the three-dimensional piece of cardiac tissue is constructed mathematically in MATLAB. The piece of heart tissue is surrounded by a conductive bath. A stimulus current is applied at one node within the tissue, the location of which does not change throughout the simulations. The development and progression of the electrical activity, initiated by the stimulus, is simulated with the bidomain model. To alternate the thickness of the tissue, the dimension in the z-direction was manually altered and the script was re-run to produce an action potential that corresponded to that exact thickness. The dimensions in the x-direction and y-direction were kept equal and remained the same throughout the simulations for simplicity.

3.4 Statistical Analysis

A one-way ANOVA test was run to examine if there was a significant difference between the action potentials that resulted from pieces of tissue with different thicknesses. The array of the membrane potential values at each time point was saved from each time the script was run with a different thickness. Each set of membrane potential values was inserted into a single column in

JMP, and the one-way ANOVA test measured the differences between each set. The resulting p-value was used as the determining factor as to whether the membrane potential values at each time were significantly different between each run with a different tissue thickness.

Chapter 4

RESULTS

The use of the bidomain model in combination with the Beeler Reuter model for replicating the effects of hypertrophic cardiomyopathy on the action potential of a ventricular myocyte was investigated. The bidomain model was incorporated to construct the geometry of and describe the electrical conductivity of the tissue. The Beeler Reuter model was incorporated to describe the ionic current activity at each node. The two models were combined in MATLAB. The output of the model was the action potential, represented as membrane potential over time, as it propagated through the tissue model. The thickness of the tissue model was manually altered, and the membrane potential output and values were collected after each run. Phases two and three of the action potential were specifically investigated to observe whether they prolonged (evidence of hypertrophic cardiomyopathy). This active model was compared to a passive model, as well as to a Beeler Reuter model found in the literature [9], for validation.

4.1 Simulating Electrical Activity of a 3D Model of Ventricular Tissue

An action potential was created at tissue thicknesses of 5, 6, 7, 8, 9, and 10 nodes. The elapsed time was kept at 500 milliseconds for each run to simplify the visual comparison between the action potentials for each thickness. An overlay of all action potential runs can be seen in Figure 4.7.

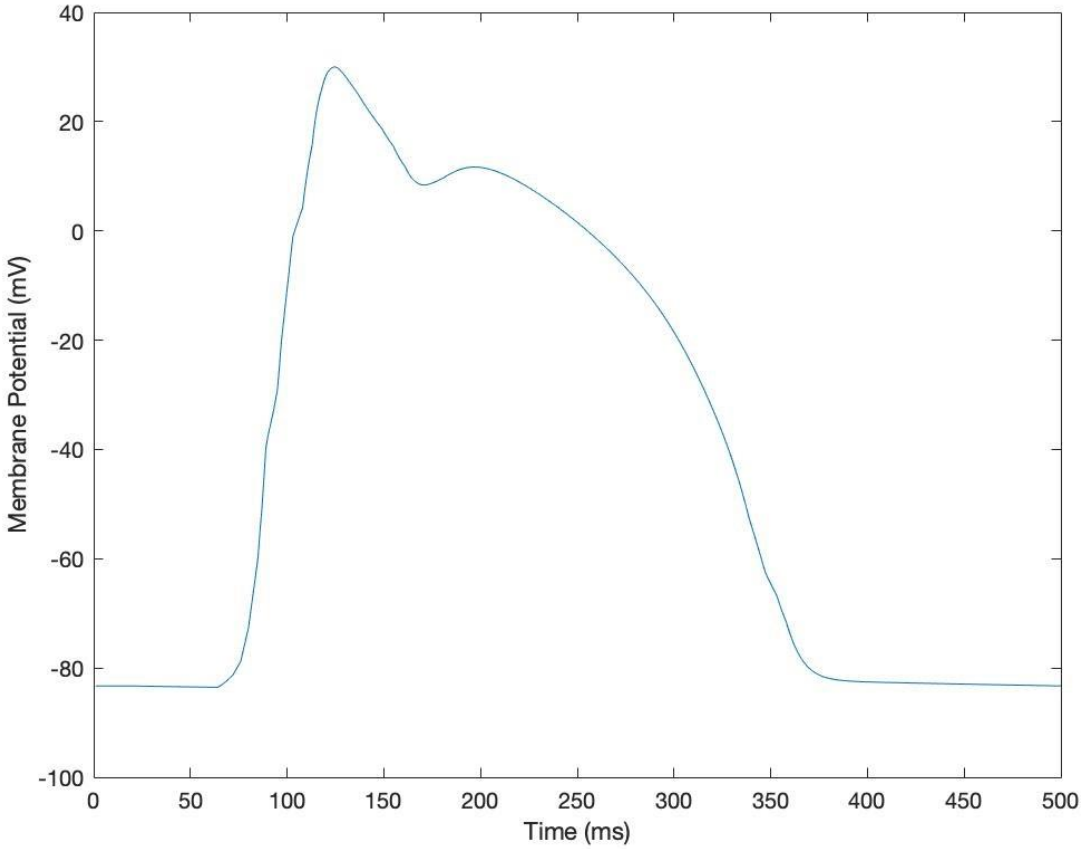

Figure 4.1. The action potential of the tissue with a thickness of 5 nodes.

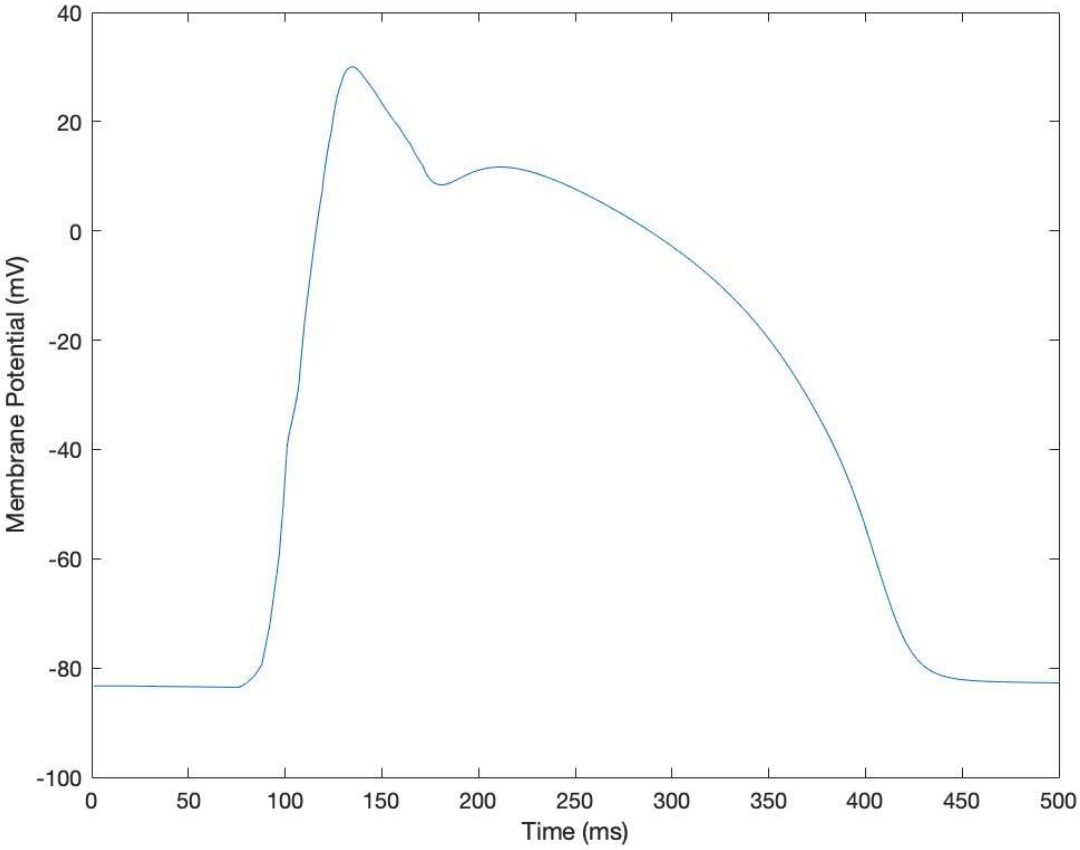

Figure 4.2. The action potential of the tissue with a thickness of 6 nodes.

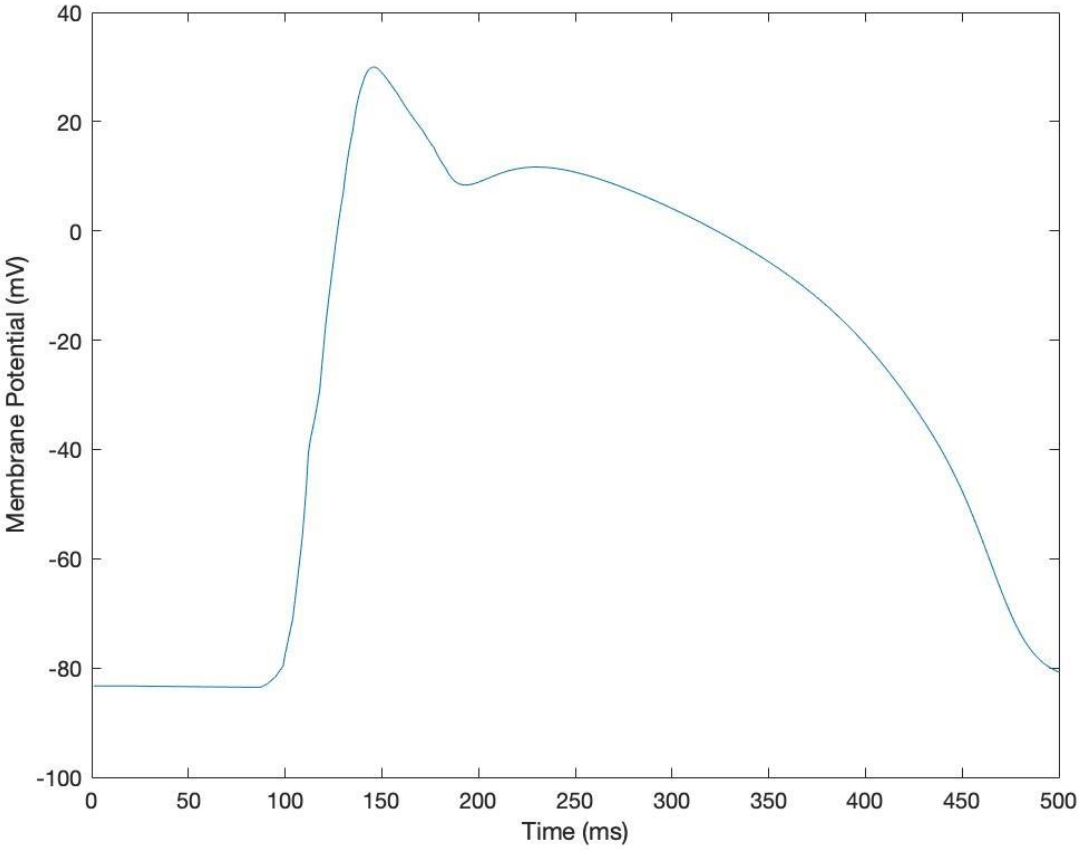

Figure 4.3. The action potential of the tissue with a thickness of 7 nodes.

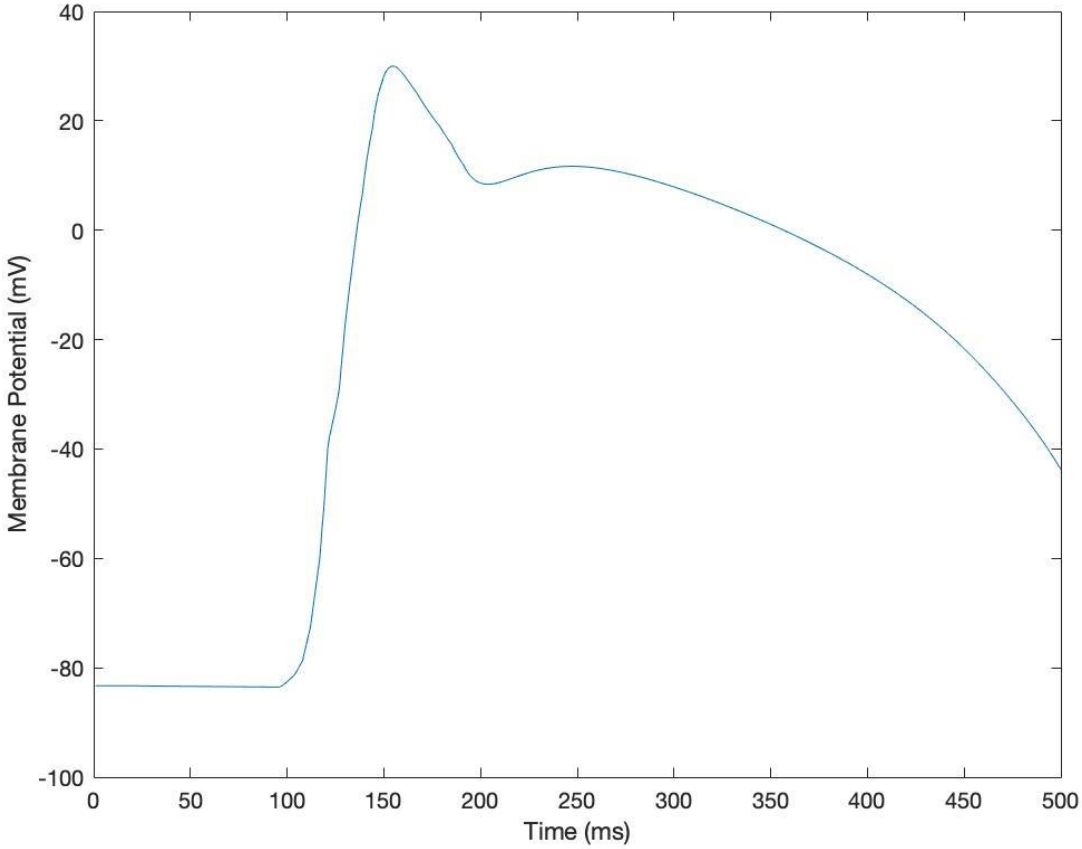

Figure 4.4. The action potential of the tissue with a thickness of 8 nodes.

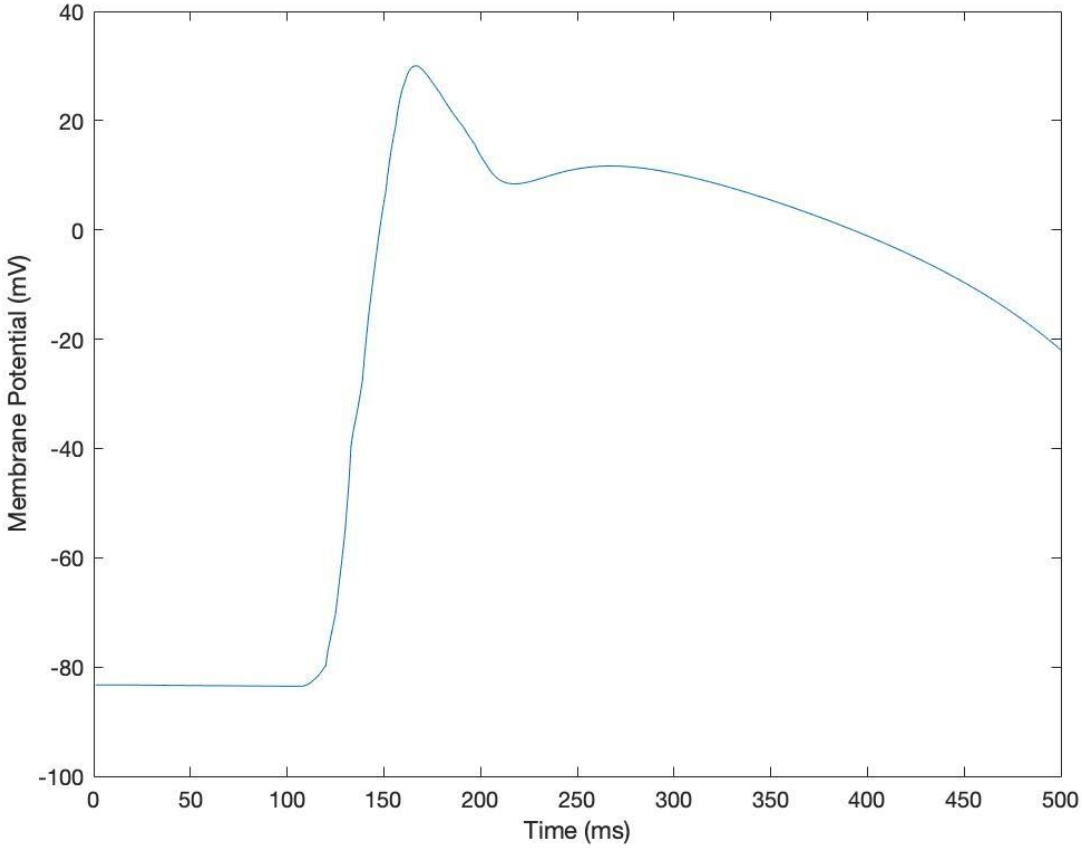

Figure 4.5. The action potential of the tissue with a thickness of 9 nodes.

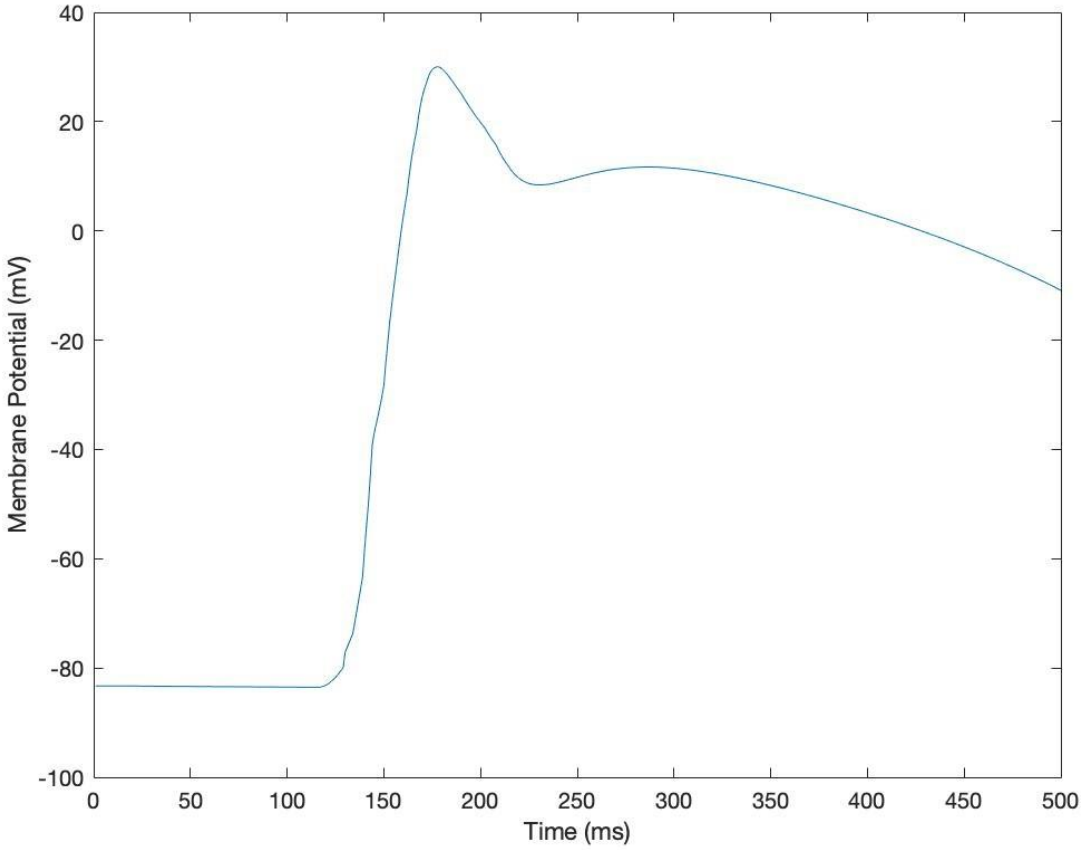

Figure 4.6. The action potential of the tissue with a thickness of 10 nodes.

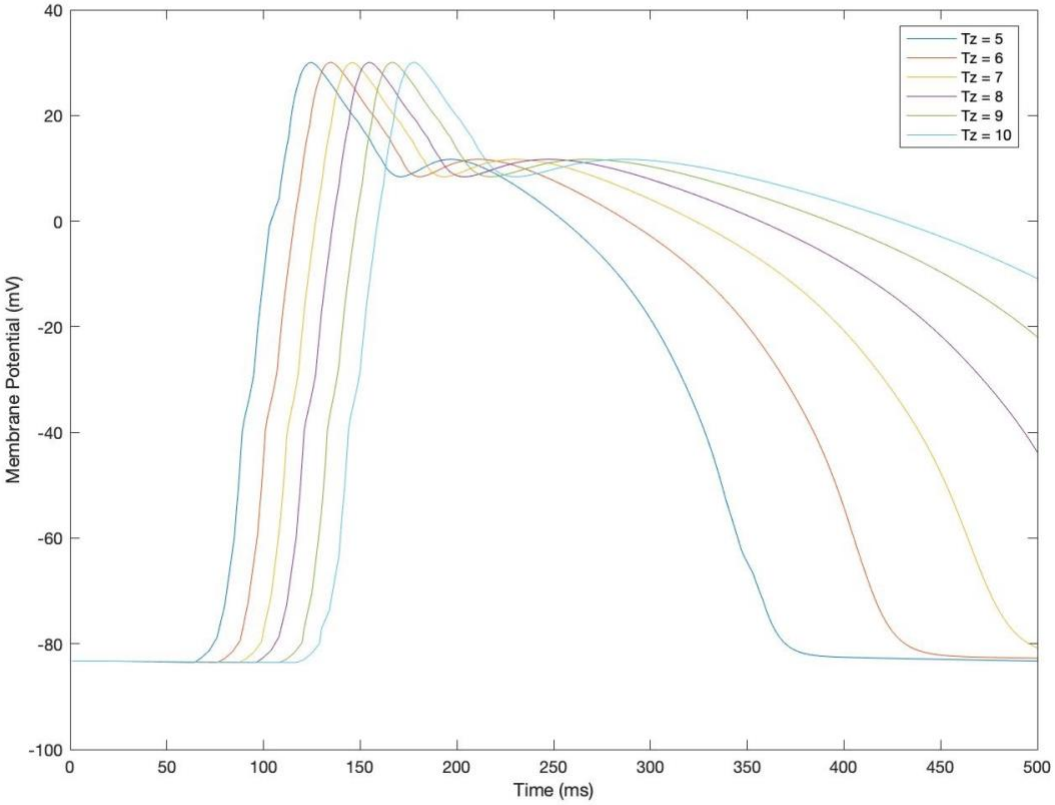

Figure 4.7. The overlaid action potentials of all tissue thicknesses.

4.2 Model Validation

For this simulation, three forms of validation were utilized in order to first validate the effect of the stimulation current within the model; then to validate the shape of the action potential; and finally, to validate the electrical components (of the bidomain model) representation of the physiological components. For validating the effectiveness of the stimulation current present within the model, it was sufficient to compare the model output, which is considered to be an “active” model due to the presence of a stimulation current, with the output of a “passive” model, wherein there is no stimulation current present. This validation technique verified the effect of the stimulus current on the action potential. In Figure 4.8, the passive model was simulated by omitting the stimulation current from the ionic current script in MATLAB. While there

is no stimulation current present, the membrane potential is still changing over time. The reason for this continual change in membrane potential over time is theorized to be a result of the continuation of the four ionic currents present within the Beeler Reuter model being held at steady state where no external stimulus is applied.

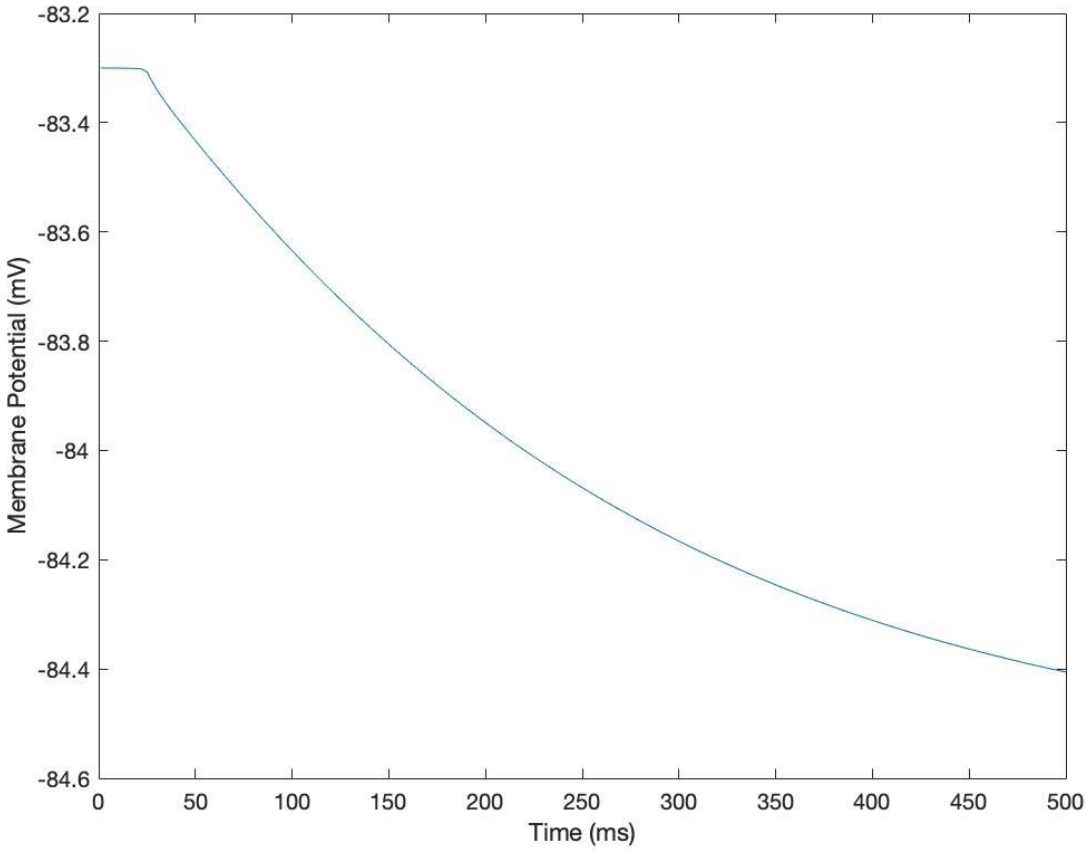

Figure 4.8. Membrane potential over time described by a passive model where the stimulation current was omitted.

The shape of the model was validated by visually comparing it to a plot of membrane potential over time produced by the Beeler Reuter model found in the literature. Figure 4.9 shows the membrane potential over time as it is produced by the Beeler Reuter model from Beeler et. al [9].

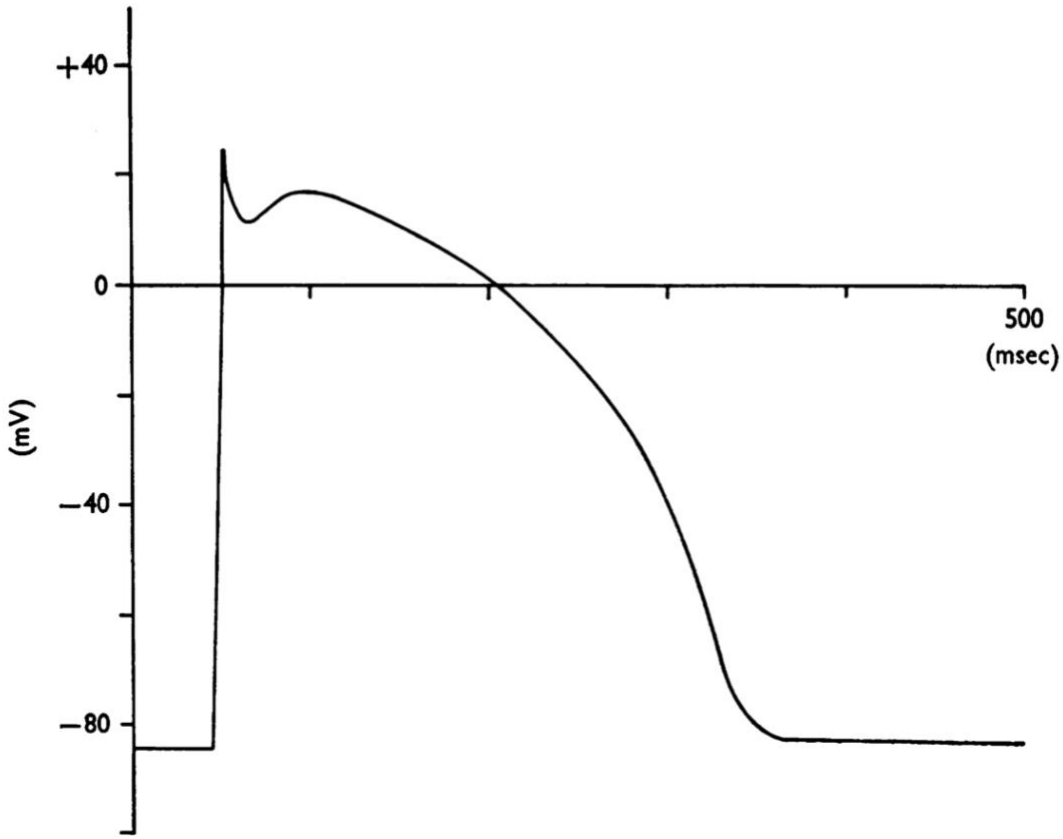

Figure 4.9. A standard action potential described by the Beeler Reuter model found in the literature [9].

Public access to clinical data such as human action potential dynamics, including those taken from cardiac tissue cells, is scarce or limited by practical or ethical concerns [10]. For this reason, the simulation described in this paper was not validated through experimental data. However, computational modeling based on experimental data is an important component in cardiac electrophysiological research and has been used to test a variety of mechanistic hypotheses [10].

The accuracy of the electrical representation of the physiological components is validated by describing the role of gap junctions, how they are affected during hypertrophic cardiomyopathy, and how their electrical equivalents predispose a prolonged action potential during cases of hypertrophy. The lengthening of the ventricular action potential is commonly observed in both cardiac hypertrophy and failure. Hypertrophic cardiomyopathy in the ventricles is

known to delay the recovery of excitability and is also associated with altered electronic coupling between cells, slowed conduction, and a dispersion of refractoriness. There is evidence of diminished outward current during hypertrophy which leads to action potential prolongation. Currently, an understanding of mechanisms underlying hypertrophic action potential prolongation is limited and, as a result, the means of treating hypertrophy-associated action potential prolongation is also limited.

Gap junctions provide a chemical and electrical connection between cardiac cells, allowing a coordinated action potential propagation. They determine how much depolarizing current passes from excited to non-excited regions of the network. In an adult myocardium, a given cardiomyocyte is typically electrically coupled to about 10-11 adjacent cells with gap junctions being predominantly localized at the intercalated discs at the ends of the rod-shaped cells [27]. The geometry of the interconnected cells and the number, size, and location of gap junction plaques between them all dictate the conductive properties of those cells. The area of the plaque within the gap junction directly impacts the conduction velocity of an action potential propagating from one cell to the next [28]

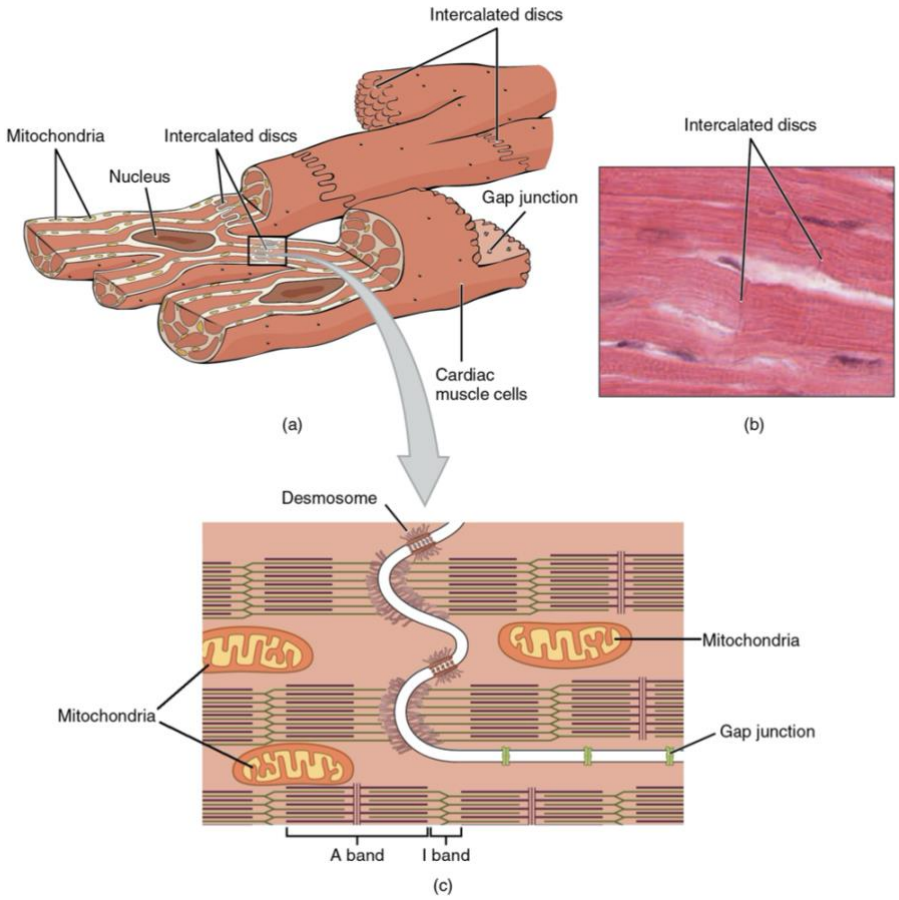

Figure 4.10. (a) Coupled cardiomyocytes. (b) Intercalated discs from a section of stained cardiac tissue. (c) Gap junctions between cardiomyocytes [11]

Gap junction remodeling has been found to precede virtually all cardiac diseases predisposing to arrhythmias. In hypertrophic ventricles in particular, the reduction of gap junction plaque area per intercalated disc is more widespread than in other types of cardiac disease [28]. A decrease in gap junction plaque area correlates with a decrease in conduction velocity, leading to a prolonged action potential.

As previously stated in section 3.2, the bidomain model is composed of a network of resistors representing the extracellular membrane and another network of resistors representing the intracellular membrane coupled by a series of a resistor and a capacitor in parallel. A diagram of a two-dimensional bidomain model can be seen in Figure 4.11.

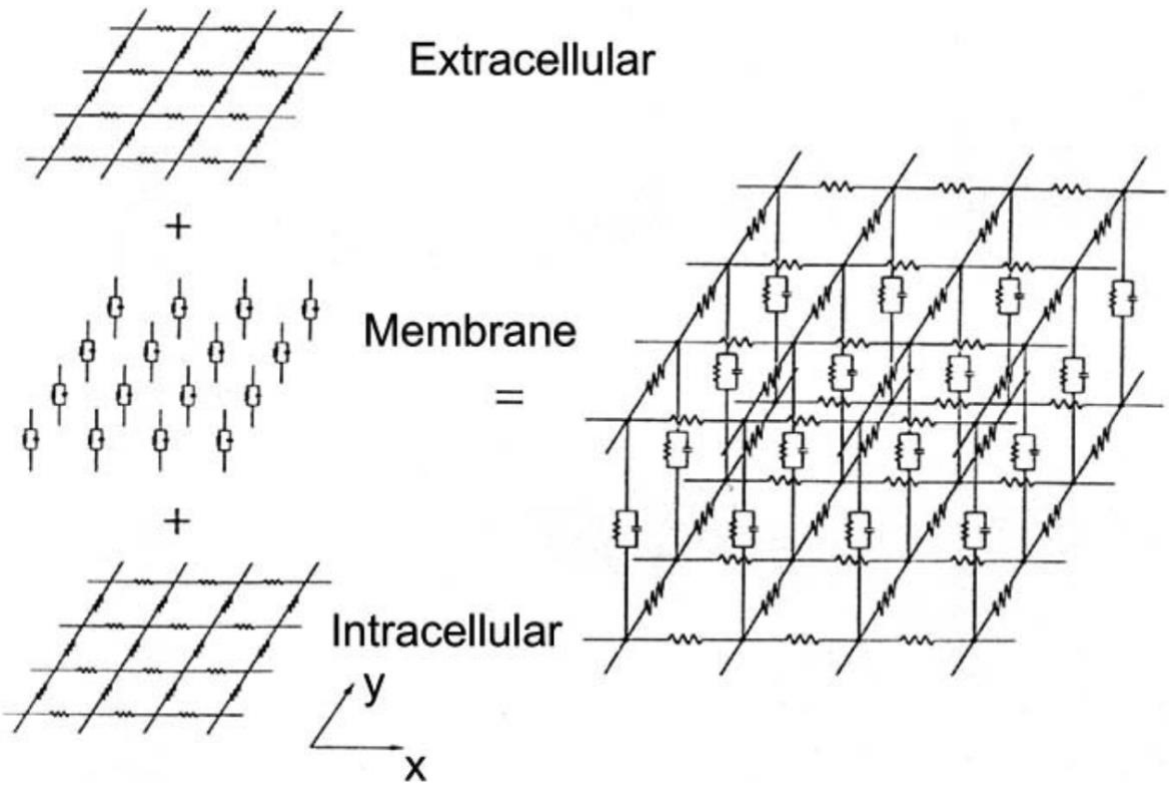

Figure 4.11. Two-dimensional bidomain network [29].

A true working myocardium is regarded as a three-dimensional network of coupled excitable elements [27]. The resistor and capacitor in parallel are analogous to the gap junction between cardiomyocytes. Altering the resistance in this parallel combination can impede the conduction of electrical signals, which equates to altering the flow of current through gap junctions [30].

Increasing the resistance in parallel with the conductance will slow the conduction velocity of the action potential. This correlates with why the latter half of the action potential becomes more and more prolonged as the tissue thickens. Additionally, as the tissue thickens, the resistance will increase in the z-direction of the tissue, making it progressively more difficult for an action potential to propagate laterally.

4.3 Statistical Analysis

A one-way ANOVA test was run in JMP to determine if any of the data sets were significantly different from one another. The test results yielded a p-value of <0.0001 and an F ratio of 23.6962. Therefore, the null hypothesis can be rejected, and it can be confidently stated that at least one of the groups means differs from the rest. In other words, the tissue size statistically affects the shape of the action potential as it propagates through the tissue membrane. In Figure 4.12, the mean membrane potential and first standard deviation for each group is designated by a green rhombus.

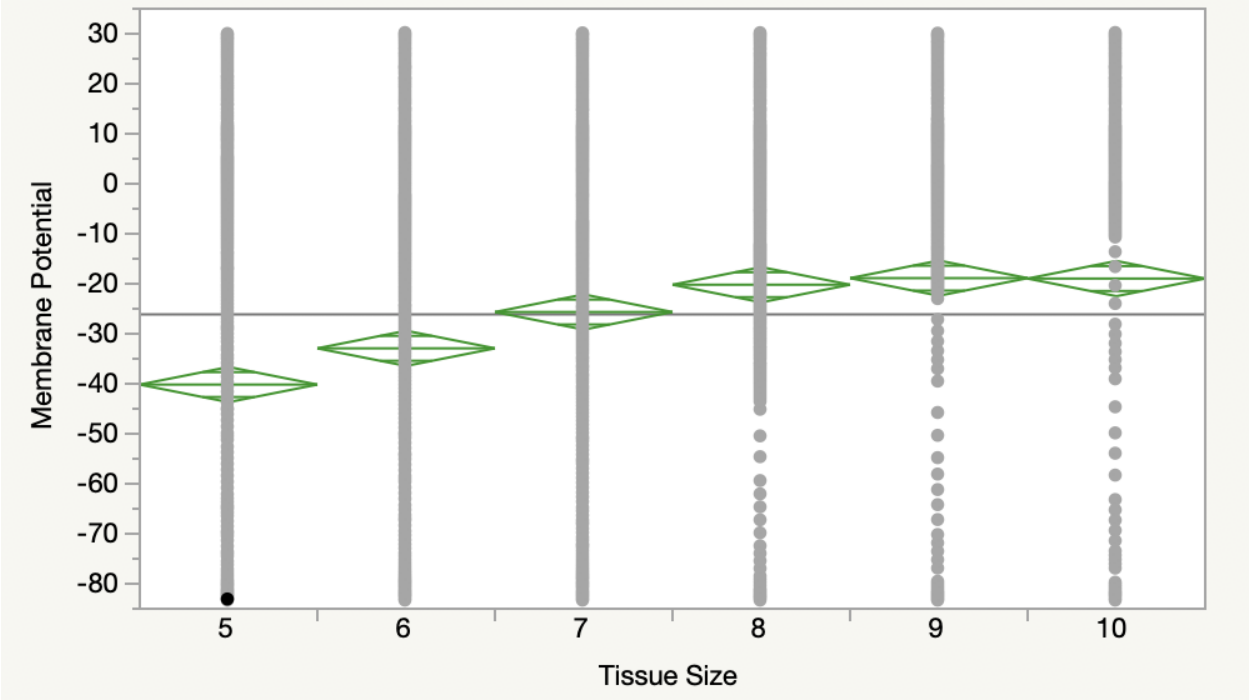

Figure 4.12. The average membrane potential values for tissue sizes of 5 nodes, 6 nodes, 7 nodes, 8 nodes, 9 nodes, and 10 nodes thickness.

Oneway Anova

Summary of Fit

Rsquare	0.038066
Adj Rsquare	0.03646
Root Mean Square Error	40.17555
Mean of Response	-26.1283
Observations (or Sum Wgts)	3000

Analysis of Variance

Source	DF	Sum of Squares	Mean Square	F Ratio	Prob > F
Tissue Size	5	191236.8	38247.4	23.6962	<.0001*
Error	2994	4832539.1	1614.1		
C. Total	2999	5023775.9			

Means for Oneway Anova

Level	Number	Mean	Std Error	Lower 95%	Upper 95%
5	500	-40.164	1.7967	-43.69	-36.64
6	500	-32.917	1.7967	-36.44	-29.39
7	500	-25.654	1.7967	-29.18	-22.13
8	500	-20.193	1.7967	-23.72	-16.67
9	500	-18.877	1.7967	-22.40	-15.35
10	500	-18.963	1.7967	-22.49	-15.44

Std Error uses a pooled estimate of error variance

Figure 4.13. Results from the one-way ANOVA test between each set of membrane potential values from each tissue thickness. The p-value is <0.0001 and the F Ratio value is 23.6962.

Chapter 5

DISCUSSION

This work explored the use of a computational model for investigating changes in the shape of a cardiac action potential brought on by ventricular tissue thickness changes from hypertrophic cardiomyopathy. It was originally hypothesized that the computational model would be able to successfully correlate an increase in ventricular tissue thickness with a prolonged cardiac action potential. It is known that specifically phases two and three of the cardiac action potentials elongate in cases of hypertrophic cardiomyopathy (Figure 2.5 indicates each phase of the cardiac action potential). These phases were visually investigated as a part of confirming the correlation. The model successfully predicted that an increase in ventricular wall thickness correlates with a prolonged action potential duration. A one-way ANOVA analysis revealed that at least one of the action potentials propagating through a piece of ventricular wall tissue was significantly different from the action potentials propagating through ventricular walls with different thicknesses. The identification of a relationship between cardiac tissue thickness and action potential shape lends insight into how electrical signal transmission can change during the progression of cardiac disease.

5.1 Implications

This model is useful because it analyzes the mechanisms by which an electric field interacts with cardiac tissue as the tissue increases in size, such as in the case of hypertrophic cardiomyopathy. This analysis shows how an action potential will propagate in the case of HCM, lending insight into how long it will take for the heart to fully contract as its ventricular tissue thickness increases.

The validation demonstrated that there is a difference between the active and passive ionic models implemented with the bidomain model, meaning that the stimulus current was appropriate and has an impact on the resulting action potential. The validation further showed

that there is a significant difference between the action potential measurement stemming from pieces of ventricular tissue with differing thicknesses.

In the medical field, there is a need for improving the specialized treatment of cardiac diseases and arrhythmias by tailoring therapy so that it is unique to each patient. This model can serve as a steppingstone for creating more in-depth models that will be able to predict the specific electrical behavior of each patient's heart by incorporating their individual cardiac geometry or ionic current fluctuations into the model. Such a model could reveal how patients may respond to treatment as no two hearts are the same. It is a non-invasive, efficient preliminary model to examine how patients may respond to treatment based on their unique cardiac geometry or ionic current dynamics.

5.2 Limitations

The major limitations of this model can be summarized by three main points: a lack of computational power to implement more complex ionic models; restricted access to experimental data on cardiac action potential dynamics to further validate the model; and assuming continuum behavior throughout the hypertrophied cardiac tissue.

As the complexity of ionic models increases, the accuracy of such ionic models also increases. The Beeler Reuter model, while useful, was created in 1977 and currently stands as one of the simpler ionic models with only 8 state variables. In recent years, ionic models have been developed that incorporate more ionic currents with some models having up to 67 state variables [31]. These complex models are more able to provide an accurate representation of the true ionic conductance inside of a cardiomyocyte. However, with more state variables in these complex models comes a demand for greater computational power. For this study, a simple ionic model was selected to reduce computational demand, even though this limited the accuracy of the ionic behavior within a cardiomyocyte.

After conducting a thorough literature review, it was discovered that there is very limited access to any experimental data describing the dynamic behavior of cardiac tissue at the cellular

level. This kind of information is challenging to collect and is not readily available to the public by practical or ethical concerns [10].

Continuum behavior was assumed for simplicity, but continuum behavior is not entirely depictive of diseased tissue. Since the progression of a disease is not regulated, the electrical behavior is not uniform throughout the entire tissue and tends to short in diseased areas.

5.3 Future Work

The work done to evaluate influential parameters within this model could be expanded upon in the future. It may be useful to investigate the quantitative relationships between tissue thickness and the length of the plateau phase of the cardiac action potential to further validate the effect of the tissue thickness on the length of the plateau phase. One could find the area under the curve of each individual output in Figure 4.7 and compare those values in a statistical analysis. A suggested statistical analysis to use in the future would be a conjoint analysis, which provides more information than a one-way ANOVA test. A conjoint analysis is traditionally used in marketing research, but it would be beneficial to consider using in order to determine how different parameters influence membrane potential.

Another example of future work in this area would be to incorporate different ionic models other than the Beeler Reuter model to investigate if and how that would change the shape of the action potential during hypertrophic cardiomyopathy. Given that their computer has enough processing power, future researchers could combine human models, such as the Ten Tusscher [36] or Iyer Mazhari Winslow [37] models, with the three-dimensional bidomain model to study the human heart's electrical behavior during hypertrophic cardiomyopathy. Human models, as opposed to generic models, are inherently more accurate in predicting the electrical behavior of human cardiac tissue and would thus be a closer representation of the true electrical behavior in diseased or non-diseased tissue.

The study performed in this thesis can be further validated by conducting an in vitro study to confirm the electrical behavior of hypertrophied cardiac tissue. Artificial hypertrophy (through mechanical stretch) could be performed on bovine cardiac tissue using a technique similar to that

described in the paper by Ovchinnikova et al [2]. It would be challenging to obtain human cardiac tissue, so bovine cardiac tissue would be recommended as it would be more readily available and perform similarly to that of human cardiac tissue.

A common technique that was found in the previous literature that was not utilized in this paper was the fluctuation of ionic current concentrations to examine how the electrical behavior of the heart changed. The concentration of each ionic current has been previously found to impact the electrical activity, but it hasn't yet been investigated for the case of hypertrophic cardiomyopathy. Altering the ionic current concentrations in the computational model for HCM or another cardiac disease would be beneficial as it is another avenue towards gaining insight on how the ionic concentrations affect the dynamics of the electrical behavior in the heart. A future investigation of potential interest could lie in creating a computational model of myocyte electrophysiology with an integration of and emphasis on Ca^{2+} transient dynamics. An integrative model of myocyte electromechanics has potential in the realm of FHC research for several reasons, the most prominent of which being that many FHC mutations are associated with high risk for lethal arrhythmias and the myocyte is the simplest system to observe in which sarcomeric mutations could exert an effect on electrical activity in the heart. Myocytes are the simplest cells to experimentally prepare and observe the effects of FHC mutations on twitch characteristics. A computational biophysically detailed electrical myocyte model could be created to validate the effects of Ca^{2+} transient current on cardiac muscle twitch in vitro.

For an in vitro study, a new approach being explored at present is to create induced pluripotent stem cells from human somatic tissues that can be differentiated into heart cells. Myocytes derived from patients harboring FHC mutations could then be used for functional cell-scale assays or as a means of obtaining mutant proteins for molecular studies. An emerging trend from similar studies has revealed that mutations linked to HCM tend to increase Ca^{2+} sensitivity of the myofilaments, while the small number of mutations linked to dilated cardiomyopathy (DCM) tend to decrease it. It seems unlikely that a single parameter would be able to describe a multi-dimensional phenotypic space of FHC, but the sensitivity of Ca^{2+} would still be useful to look into with regards to its impact on electrical dynamics related to HCM.

5.4 Conclusions

The use of this computational model could improve clinical research efforts by serving as a form of validation for conducting in vitro experiments on hypertrophied cardiac tissue to gain a better understanding of the root mechanisms of hypertrophic cardiomyopathy or related cardiac diseases. By being able to input model parameters that are specific to patients' cardiac geometry, personalized treatment can be delivered to better target and advance the recovery of cardiac diseases such as hypertrophic cardiomyopathy.

BIBLIOGRAPHY

[1] Passini, Elisa, et al. “Mechanisms of pro-Arrhythmic Abnormalities in Ventricular Repolarization and Anti-Arrhythmic Therapies in Human Hypertrophic Cardiomyopathy.” *Journal of Molecular and Cellular Cardiology*, Academic Press, July 2016, www.ncbi.nlm.nih.gov/pmc/articles/PMC4915817/.

[2] Ovchinnikova, Ekaterina, et al. “Modeling Human Cardiac Hypertrophy in Stem Cell-Derived Cardiomyocytes.” *Stem Cell Reports*, vol. 10, no. 3, 2018, pp. 794–807., doi:10.1016/j.stemcr.2018.01.016.

[3] Frey, Norbert, et al. “Hypertrophy of the Heart.” *Circulation*, vol. 109, no. 13, 2004, pp. 1580–1589., doi:10.1161/01.cir.0000120390.68287.bb.

[4] Ibrahim, Adebisi O., et al. “Dynamical Modelling of Cardiac Electrical Activity Using Bidomain Approach: The Effects of Variation of Ionic Model Parameters.” *Journal of Biomedical Science and Engineering*, vol. 06, no. 06, 2013, pp. 598–608., doi:10.4236/jbise.2013.66076.

[5] Chang, Eugene Tze-Yeng. “Towards Understanding the Electrogram: Theoretical & Experimental Multiscale Modelling of Factors Affecting Action Potential Propagation in Cardiac Tissue.” *Imperial College London*, 2013.

[6] Tanyous, Fred (Farid). “Mapping Electrical Propagation in the Cardiac Sinoatrial Node: An Experimental and Computational Modelling Approach.” *The University of New South Wales*, 2019.

[7] Bantle, Annabel Christin. “Mathematically Modeling the Electrical Activity of a Wedge of Left Ventricular Heart Tissue.” *Aalborg University*, 2019.

[8] Marian, Ali J, and Eugene Braunwald. “Hypertrophic Cardiomyopathy: Genetics, Pathogenesis, Clinical Manifestations, Diagnosis, and Therapy.” *Circulation research* vol. 121,7 (2017): 749-770. doi:10.1161/CIRCRESAHA.117.311059

[9] Beeler, G W, and H Reuter. “Reconstruction of the action potential of ventricular myocardial fibres.” *The Journal of physiology* vol. 268,1 (1977): 177-210. doi:10.1113/jphysiol.1977.sp011853

[10] Gray, Richard A., and Michael R. Franz. “A Model for Human Action Potential Dynamics in Vivo.” *American Journal of Physiology-Heart and Circulatory Physiology*, vol. 318, no. 3, 2020, doi:10.1152/ajpheart.00557.2019.

[11] L. Biga, S. Dawson, A. Harwell, R. Hopkins, J. Kaufmann, M. LeMaster, P. Matern, K. Morrison-Graham, D. Quick, J. Runyeon, and L. Whittier, Anatomy Physiology. Open Oregon State, Oregon State University, 2018.

[12] Sigg, Daniel C. *Cardiac Electrophysiology Methods and Models*. Springer, 2010.

[13] Wei, Xingyu. “Physiology, Cardiac Repolarization Dispersion and Reserve.” *StatPearls [Internet].*, U.S. National Library of Medicine, 30 Apr. 2020, www.ncbi.nlm.nih.gov/books/NBK537194/.

[14] “Anatomy and Function of the Heart's Electrical System.” *Johns Hopkins Medicine*, www.hopkinsmedicine.org/health/conditions-and-diseases/anatomy-and-function-of-the-hearts-electrical-system.

[15] Campbell, Stuart G., and Andrew D. McCulloch. “Multi-Scale Computational Models of Familial Hypertrophic Cardiomyopathy: Genotype to Phenotype.” *Journal of The Royal Society Interface*, vol. 8, no. 64, 2011, pp. 1550–1561., doi:10.1098/rsif.2011.0184.

[16] Bers, D. Cardiac excitation–contraction coupling. *Nature* 415, 198–205 (2002). https://doi.org/10.1038/415198a

[17] Nerbonne JM, Kass RS. Molecular physiology of cardiac repolarization. Physiol Rev. 2005 Oct;85(4):1205-53. doi: 10.1152/physrev.00002.2005. PMID: 16183911.

[18] Abdul Kadir, Lina, et al. “Emerging Roles of the Membrane Potential: Action Beyond the Action Potential.” *Frontiers*, Frontiers, 2 Nov. 2018, www.frontiersin.org/articles/10.3389/fphys.2018.01661/full.

[19] Webster, John G. *Medical Instrumentation: Application and Design*. J. Wiley & Sons, 1998.

[20] Cha, Chae Young, and Akinori Noma. “Steady-State Solutions of Cell Volume in a Cardiac Myocyte Model Elaborated for Membrane Excitation, Ion Homeostasis and Ca^{2+} Dynamics.” *Journal of Theoretical Biology*, vol. 307, 11 May 2012, pp. 70–81., doi:https://doi-org.ezproxy.lib.calpoly.edu/10.1016/j.jtbi.2012.04.025.

[21] Aulakh, M. Why old heart cells don't multiply. *Nat Rep Stem Cells* (2009). https://doi.org/10.1038/stemcells.2009.31

[22] Gordon F. Tomaselli, Eduardo Marbán, Electrophysiological remodeling in hypertrophy and heart failure, *Cardiovascular Research*, Volume 42, Issue 2, May 1999, Pages 270–283, https://doi.org/10.1016/S0008-6363(99)00017-6

[23] Coltart DJ, Meldrum SJ. Hypertrophic cardiomyopathy. An electrophysiological study. Br Med J. 1970 Oct 24;4(5729):217-8. doi: 10.1136/bmj.4.5729.217. PMID: 5528752; PMCID: PMC1819778.

[24] Gerdes, A.Martin. “Cardiac Myocyte Remodeling in Hypertrophy and Progression to Failure.” *Journal of Cardiac Failure*, vol. 8, no. 6, 2002, doi:10.1054/jcaf.2002.129280.

[25] Tirziu, D. “Cardiac Hypertrophy: Signaling and Cellular Crosstalk.” *Encyclopedia of Cardiovascular Research and Medicine*, 2018, pp. 434–450., doi:10.1016/b978-0-12-809657-4.99834-x.

[26] Takeda, Norifumi, and Ichiro Manabe. “Cellular Interplay between Cardiomyocytes and Nonmyocytes in Cardiac Remodeling.” *International Journal of Inflammation*, vol. 2011, 2011, pp. 1–13., doi:10.4061/2011/535241.

[27] “Beeler-Reuter Model of Ventricular Myocardial Action Potential.” *University of Rhode Island*, 2006.

[28] Boulakia, Muriel, et al. “Mathematical Modeling of Electrocardiograms: A Numerical Study.” *Annals of Biomedical Engineering*, vol. 38, no. 3, 2009, pp. 1071–1097., doi:10.1007/s10439-009-9873-0.

[29] Efimov, Igor R, et al., editors. *Cardiac Bioelectric Therapy: Mechanisms and Practical Implications*. SPRINGER, 2009.

[30] Sundnes J, Nielsen BF, Mardal KA, Cai X, Lines GT, Tveito A. On the computational complexity of the bidomain and the monodomain models of electrophysiology. Ann Biomed Eng. 2006 Jul;34(7):1088-97. doi: 10.1007/s10439-006-9082-z. Epub 2006 May 16. PMID: 16773461.

[31] H. I. Saleheen and K. T. Ng, "A new three-dimensional finite-difference bidomain formulation for inhomogeneous anisotropic cardiac tissues," in *IEEE Transactions on Biomedical Engineering*, vol. 45, no. 1, pp. 15-25, Jan. 1998, doi: 10.1109/10.650347.

[32] Rohr, S. “Role of Gap Junctions in the Propagation of the Cardiac Action Potential.” *Cardiovascular Research*, vol. 62, no. 2, 2004, pp. 309–322., doi:10.1016/j.cardiores.2003.11.035.

[33] Jongsma, Habo J., and Ronald Wilders. “Gap Junctions in Cardiovascular Disease.” *Circulation Research*, vol. 86, no. 12, 2000, pp. 1193–1197., doi:10.1161/01.res.86.12.1193.

[34] J. Roth, Bradley. “Numerical Simulations of Cardiac Tissue Excitation and Pacing Using the Bidomain Model.” *The Open Pacing, Electrophysiology & Therapy Journal*, vol. 4, no. 1, 2011, pp. 1–9., doi:10.2174/1876536x01104010001.

[35] Robinson, Martha M et al. “Modeling biological membranes with circuit boards and measuring electrical signals in axons: student laboratory exercises.” *Journal of visualized experiments : JoVE* ,47 2325. 18 Jan. 2011, doi:10.3791/2325

[36] Ten Tusscher, K. H., et al. “A Model for Human Ventricular Tissue.” *American Journal of Physiology-Heart and Circulatory Physiology*, vol. 286, no. 4, 2004, doi:10.1152/ajpheart.00794.2003.

[37] Iyer V, Mazhari R, Winslow RL. A computational model of the human left-ventricular epicardial myocyte. Biophys J. 2004 Sep;87(3):1507-25. doi: 10.1529/biophysj.104.043299. PMID: 15345532; PMCID: PMC1304558.

```
%%%%%%%%%%%%%%%%%%%%%%%%%%%%%%%%%%%%%%%%%%%%%%%%%%%%%%%%%%%%%%%%%%%%%%%%%%
%%%%%%%
%
%   Function:       BR_Prime
%   Revision Date:  11/16/2020
%   Author:         Socrates Dokos
%   Co-Author:      Julia Kelley
%
%   Function for solving the Beeler-Reuter (1977) model. For use with
%   ode15s.
%
%   Arguments:     t   = time (ms)
%
%                  y   = vector of initial values for membrane
potential (V),
%                        calcium concentration (Ca), and governing
parameters
%                        (x1, m, h, j, d, and f)
%
%   Returns:       y_prime   = vector of approximated values for
membrane
%                              potential (V), calcium concentration
(Ca),
%                              and governing parameters(x1, m, h, j, d,
and f)
%
%%%%%%%%%%%%%%%%%%%%%%%%%%%%%%%%%%%%%%%%%%%%%%%%%%%%%%%%%%%%%%%%%%%%%%%%%%
%%%%%%%

function y_prime = BR_Prime(t,y)

global Cm r_Ca Ca_SR k_up A_K1 A_x1 g_Na g_NaC V_Na g_s A_s t_on t_dur;
y_prime = zeros(8,1);

V = y(1);
Ca = y(2);
x1 = y(3);
m = y(4);
h = y(5);
j = y(6);
d = y(7);
f = y(8);

alpha_x1 = 0.0005*exp(0.083*(V+50))/(exp(0.057*(V+50))+1);
beta_x1 = 0.0013*exp(-0.06*(V+20))/(exp(-0.04*(V+20))+1);

alpha_m = -(V+47)/(exp(-0.1*(V+47))-1);
beta_m = 40*exp(-0.056*(V+72));

alpha_h = 0.126*exp(-0.25*(V+77));
beta_h = 1.7/(exp(-0.082*(V+22.5))+1);

alpha_j = 0.055*exp(-0.25*(V+78))/(exp(-0.2*(V+78))+1);
```

```
beta_j = 0.3/(exp(-0.1*(V+32))+1);

alpha_d = 0.095*exp(-0.01*(V-5))/(exp(-0.072*(V-5))+1);
beta_d = 0.07*exp(-0.017*(V+44))/(exp(0.05*(V+44))+1);

alpha_f = 0.012*exp(-0.008*(V+28))/(exp(0.15*(V+28))+1);
beta_f = 0.0065*exp(-0.02*(V+30))/(exp(-0.2*(V+30))+1);

V_Ca = -82.3 - 13.0287*log(Ca);


i_K1 = A_K1*(4*(exp(0.04*(V+85))-
1)/(exp(0.08*(V+53))+exp(0.04*(V+53)))+
      0.2*(V+23)/(1-exp(-0.04*(V+23))));
i_x1 = A_x1*x1*(exp(0.04*(V+77))-1)/exp(0.04*(V+35));
i_Na = (g_Na*m^3*h*j+g_NaC)*(V-V_Na);


i_s = g_s*d*f*(V-V_Ca);



if((t>= t_on)&&(t<t_on+t_dur))


    i_stim = A_s;
else
    i_stim = 0;
end

% active model:
% y_prime(1) = -(1/Cm)*(i_K1 + i_x1 + i_Na + i_s - i_stim);

% passive model:
y_prime(1) = -(1/Cm)*(i_K1 + i_x1 + i_Na + i_s);

y_prime(2) = -r_Ca*i_s+k_up*(Ca_SR - Ca);
y_prime(3) = alpha_x1*(1-x1) - beta_x1*x1;
y_prime(4) = alpha_m*(1-m) - beta_m*m;
y_prime(5) = alpha_h*(1-h) - beta_h*h;
y_prime(6) = alpha_j*(1-j) - beta_j*j;
y_prime(7) = alpha_d*(1-d) - beta_d*d;
y_prime(8) = alpha_f*(1-f) - beta_f*f;
end
```

```
%%%%%%%%%%%%%%%%%%%%%%%%%%%%%%%%%%%%%%%%%%%%%%%%%%%%%%%%%%%%%%%%%%%%%%%
%%%%%%%
%
%   Script:         BRBdiomain
%
%   Revision Date:  12/29/2020
%
%   Author:         Julia Kelley
%
%   Script for creating a 3D model of cardiac tissue by integrating the
%   Bidomain and Beeler Reuter Models.
%   Uses the BR_Prime function file as the basis of the Beeler_Retuer
model.
%
%%%%%%%%%%%%%%%%%%%%%%%%%%%%%%%%%%%%%%%%%%%%%%%%%%%%%%%%%%%%%%%%%%%%%%%
%%%%%%%

close all
clear all

% Tissue Grid
Tx = 10;                       % number of nodes in the x direction
Ty = 10;                       % number of nodes in the y direction
Tz = 5;                        % number of nodes in the z direction
TS = Tx*Ty*Tz;                 % total tissue size
ht = .2e-3;                    % distance between tissue grid points
(m)

% Bath grid (on two sides of tissue)
Bx = Tx;                       % number of nodes in the x direction
By = Ty;                       % number of nodes in the y direction
Bz = 10;                       % number of nodes in the z direction
BS = Bx*By*Bz;                 % total bath size
hb = 0.2E-3;                   % distance between bath grid points (m)

% Time Steps
t_simulation = 3;              % simulation time (ms)
delta_t = 0.02;                % size of time step (ms)
N = t_simulation/delta_t;      % number of time steps (dimensionless)

fprintf('Set up stimulus\n')

% Stimulus
Stimulus = 3E5;                % stimulus current (mA/m^2)
t_stim_on = 5;                 % start of stimulus (ms)
t_stim = 1;                    % stimulus duration (ms)
t_stim_on = t_stim_on/delta_t; % (dimensionless)
t_stim = t_stim/delta_t;       % (dimensionless)

% Stimulus point number
P = 1;                         % Stimulate at corner point location =
(0,0,0)
Istim = zeros(TS,1);           % units [mA/m^2]
```

```
Istim(P,1) = Stimulus;

% Membrane parameter
beta = 3E5;                     % surface to volume ratio (1/m)

% Conductivity
sigmax_i = 0.2;                 % intracellular conductance along fiber
                                  (x dir.) (S/m)
sigmay_i = 0.02;                % intracellular conductance vertical to
fiber
                                  (y dir.) (S/m)
sigmaz_i = 0.02;                % intracellular conductance vertical to
fiber
                                  (z dir.) (S/m)

sigmax_e = 0.2;                 % extracellular conductance along fiber
                                  (x dir.) (S/m)
sigmay_e = 0.08;                % extracellular conductance vertical to
fiber
                                  (y dir.) (S/m)
sigmaz_e = 0.08;                % extracellular conductance vertical to
fiber
                                  (z dir.) (S/m)

sigmax_b = 0.2;                 % bath conductance in x direction (S/m)
sigmay_b = 0.2;                 % bath conductance in y direction (S/m)
sigmaz_b = 0.2;                 % bath conductance in z direction (S/m)

% Laplacian matrices used to solve finite difference method (spatial
discretization)
% Boundary conditions are included in the matrices

fprintf('Laplacian matrix\n')

% Laplacian matrix for sigma_i in tissue and bath
BigM_i = spalloc(TS+2*BS,TS+2*BS,2*Tx*Ty+2*(Ty-2)*(Tz-2)+6*(Tx-2)*(Ty-
2)*(Tz-2)+2*BS);  % units: [dimensionless]

for n = 1:BS
    BigM_i(n,n) = 1;
end
for n = BS+1:BS+TS
    BigM_i(n,n) = 1;
    if n < BS+Tx*Ty+1
        for k = 1:Ty-2
            if n > BS+k*Tx+1 && n < BS + (k+1)*Tx
                BigM_i(n,n) = (-2*sigmax_i - 2*sigmay_i)/ht^2;  % units
= [S/m^3] defines the conductivity at each node point
                BigM_i(n,n-1) = sigmax_i/ht^2; % Defines the
conductivity at each point in the intracellular domain in the x
direction
                BigM_i(n,n+1) = sigmax_i/ht^2;
                BigM_i(n,n-Tx) = sigmay_i/ht^2; % Defines the
conductivity at each point in the intracellular domain in the y
direction
                BigM_i(n,n+Tx) = sigmay_i/ht^2;
```

```
            end
        end
    end
    for kk = 1:Tz-2
        for k = 1:Ty-2
            if ((n > BS+kk*Tx*Ty+k*Tx+1) && (n < BS+kk*Tx*Ty+(k+1)*Tx))
            BigM_i(n,n) = (-2*sigmax_i-2*sigmay_i-2*sigmaz_i)/ht^2;
            BigM_i(n,n-1) = sigmax_i/ht^2;
            BigM_i(n,n+1) = sigmax_i/ht^2;
            BigM_i(n,n-Tx) = sigmay_i/ht^2;
            BigM_i(n,n+Tx) = sigmay_i/ht^2;
            BigM_i(n,n-Tx*Ty) = sigmaz_i/ht^2;
            BigM_i(n,n+Tx*Ty) = sigmaz_i/ht^2;
            end
        end
    end
end
for n = BS+TS:TS+2*BS
    BigM_i(n,n) = 1;
end

% Laplacian matrix for sigma e in tissue
M_e = spalloc(TS,TS,2*Tx*Ty+2*(Ty-2)*(Tz-2)+6*(Tx-2)*(Ty-2)*(Tz-2));
for n = 1:TS
    M_e(n,n) = 1;
    if n < Tx*Ty+1
        for k = 1:Ty-2
            if n > k*Tx+1 && n < (k+1)*Tx
                M_e(n,n) = (-2*sigmax_e - 2*sigmay_e)/ht^2;
                M_e(n,n-1) = sigmax_e/ht^2;
                M_e(n,n+1) = sigmax_e/ht^2;
                M_e(n,n-Tx) = sigmay_e/ht^2;
                M_e(n,n+Tx) = sigmay_e/ht^2;
            end
        end
    end
    for kk = 1:Tz-2
        for k = 1:Ty-2
            if ((n > kk*Tx*Ty+k*Tx+1) && (n < kk*Tx*Ty+(k+1)*Tx))
                M_e(n,n) = (-2*sigmax_e-2*sigmay_e-2*sigmaz_e)/ht^2;
                M_e(n,n-1) = sigmax_e/ht^2;
                M_e(n,n+1) = sigmax_e/ht^2;
                M_e(n,n-Tx) = sigmay_e/ht^2;
                M_e(n,n+Tx) = sigmay_e/ht^2;
                M_e(n,n-Tx*Ty) = sigmaz_e/ht^2;
                M_e(n,n+Tx*Ty) = sigmaz_e/ht^2;
            end
        end
    end
end

% Laplacian Matrix for (sigma_i + sigma_e) in tissue and bath
 BigM_ie = spalloc(TS+2*BS,TS+2*BS,2*Tx*Ty+2*(Ty-2)*(Tz-2)+6*(Tx-
2)*(Ty-2)*(Tz-2)+2*BS+12*(Bx-2)*(By-2)*(Bz-2));
 for n = 1:BS
     BigM_ie(n,n) = 1;
     for kk = 1:Bz-2
```

```
        for k = 1:By-2
            if ((n > kk*Bx*By+k*Bx+1) && (n < kk*Bx*By + (k+1)*Bx))
            BigM_ie(n,n) = (-2*sigmax_b-2*sigmay_b-2*sigmaz_b)/hb^2;
            BigM_ie(n,n-1) = sigmax_b/hb^2;
            BigM_ie(n,n+1) = sigmax_b/hb^2;
            BigM_ie(n,n-Bx) = sigmay_b/hb^2;
            BigM_ie(n,n+Bx) = sigmay_b/hb^2;
            BigM_ie(n,n-Bx*By) = sigmaz_b/hb^2;
            BigM_ie(n,n+Bx*By) = sigmaz_b/hb^2;
            end
        end
    end
end
for n = BS+1:BS+TS
    BigM_ie(n,n) = 1;
    if n < BS+Tx*Ty+1
        for k = 1:Ty-2
            if n > BS+k*Tx+1 && n < BS+(k+1)*Tx
            BigM_ie(n,n) = (-(sigmax_e+sigmax_b)-(sigmay_e+sigmay_b)-
sigmaz_e-sigmaz_b)/ht^2;
            BigM_ie(n,n-1) = (sigmax_e+sigmax_b)/2*ht^2;
            BigM_ie(n,n+1) = (sigmax_e+sigmax_b)/2*ht^2;
            BigM_ie(n,n-Tx) = (sigmay_e+sigmay_b)/2*ht^2;
            BigM_ie(n,n+Tx) = (sigmay_e+sigmay_b)/2*ht^2;
            BigM_ie(n,n-Tx*Ty) = sigmaz_b/hb^2;
            BigM_ie(n,n+Tx*Ty) = sigmaz_e/ht^2;
            end
        end
    end
    for kk = 1:Tz-2
        for k = 1:Ty-2
            if ((n > BS+kk*Tx*Ty+k*Tx+1) && (n <
BS+kk*Tx*Ty+(k+1)*Tx))
                BigM_ie(n,n) = (-2*(sigmax_i+sigmax_e)-
2*(sigmay_i+sigmay_e)-2*(sigmaz_i+sigmaz_e))/ht^2;
                BigM_ie(n,n-1) = (sigmax_i+sigmax_e)/ht^2;
                BigM_ie(n,n+1) = (sigmax_i+sigmax_e)/ht^2;
                BigM_ie(n,n-Tx) = (sigmay_i+sigmay_e)/ht^2;
                BigM_ie(n,n+Tx) = (sigmay_i+sigmay_e)/ht^2;
                BigM_ie(n,n-Tx*Ty) = (sigmaz_i+sigmaz_e)/ht^2;
                BigM_ie(n,n+Tx*Ty) = (sigmaz_i+sigmaz_e)/ht^2;
            end
        end
    end
    if n > BS+Tx*Ty*(Tz-1)
       BigM_ie(n,n) = (-(sigmax_e+sigmax_b)-(sigmay_e+sigmay_b)-
(sigmaz_e+sigmaz_b))/ht^2;
       BigM_ie(n,n-1) = (sigmax_e+sigmax_b)/2*ht^2;
       BigM_ie(n,n+1) = (sigmax_e+sigmax_b)/2*ht^2;
       BigM_ie(n,n-Tx) = (sigmay_e+sigmay_b)/2*ht^2;
       BigM_ie(n,n+Tx) = (sigmay_e+sigmay_b)/2*ht^2;
       BigM_ie(n,n-Tx*Ty) = sigmaz_e/ht^2;
       BigM_ie(n,n+Tx*Ty) = sigmaz_b/hb^2;
    end
end
for n = BS+TS+1:TS+2*BS
    BigM_ie(n,n) = 1;
```

```
    for kk = 1:Bz-2
        for k = 1:By-2
            if ((n > BS+TS+(kk-1)*Bx*By+k*Bx+1) && (n < BS+TS+(kk-
1)*Bx*By+(k+1)*Bx))
            BigM_ie(n,n) = (-2*sigmax_b-2*sigmay_b-2*sigmaz_b)/hb^2;
            BigM_ie(n,n-1) = sigmax_b/hb^2;
            BigM_ie(n,n+1) = sigmax_b/hb^2;
            BigM_ie(n,n-Bx) = sigmay_b/hb^2;
            BigM_ie(n,n+Bx) = sigmay_b/hb^2;
            BigM_ie(n,n-Bx*By) = sigmaz_b/hb^2;
            BigM_ie(n,n+Bx*By) = sigmaz_b/hb^2;
            end
        end
    end
 end

 neg_BigM_ie = -BigM_ie;    % makes bicgstabl function applicable
(positive definiteness)

 fprintf('Beeler Reuter parameters\n')

 global Cm r_Ca Ca_SR k_up A_K1 A_x1 g_Na g_NaC V_Na g_s A_s t_on
t_dur;

Cm = 1;          % uC/cm^23
r_Ca = 1E-7;     % M*cm^2/nC
Ca_SR = 1E-7;    % M
k_up = 0.07;     % 1/ms
A_K1 = 0.35;     % uA/cm^2
A_x1 = 0.8;      % uA/cm^2
V_Na = 50;       % mV
g_Na = 4;        % mS/cm^2
g_NaC = 0.003;   % mS/cm^2
g_s = 0.09;      % mS/cm^2
A_s = 40;        % uA/cm^2
t_on = 50;       % ms
t_dur = 1;       % ms

Y_initial = [-83.3, 1.87E-7, 0.1644, 0.01, 0.9814, 0.9673, 0.0033,
0.9884];

options = odeset('MaxStep', 1.05);
[time, Y_out] = ode15s('BR_Prime', [0 499], Y_initial, options);
membrane_potential = Y_out(:,1);

Vhelp = zeros(TS+2*BS,1);

Vhelp(BS+1:BS+TS) = membrane_potential;

phi_e = zeros(TS,N);
Big_phi = zeros(TS+2*BS,1);
neg_Big_phi = -Big_phi;

fprintf('Bidomain solution\n')

for i = 1:N-1
[neg_Big_phi(:,1),flag] = bicgstabl(neg_BigM_ie,(BigM_i*Vhelp));
```

```
    if flag
    end

    Big_phi(:,1) = -neg_Big_phi(:,1);
    phi_e(:,1) = Big_phi(BS+1:BS+TS,1);

     if i <= t_stim
          dVmdt = (-M_e*phi_e(:,1)+Istim)/(beta*Cm)-
(membrane_potential(:,1));
      else
          dVmdt = (-M_e*phi_e(:,1))/(beta*Cm)-
(membrane_potential(:,1));
      end


      for kz = 1:Tz
          dVmdt((kz-1)*Tx*Ty+1:(kz-1)*Tx*Ty+Tx+1,1) = 0;
          dVmdt((kz-1)*Tx*Ty+(Ty-1)*Tx:(kz-1)*Tx*Ty+Tx*Ty,1) = 0;
          for ky = 2:Ty-2
              dVmdt((kz-1)*Tx*Ty+ky*Tx:(kz-1)*Tx*Ty+ky*Tx+1,1) = 0;
          end
      end


      membrane_potential(:,i+1) =
membrane_potential(:,1)+dVmdt*(delta_t/1000);
      Vhelp(BS+1:BS+TS) = membrane_potential(:,i+1);
end
```